CRYSTAL GROWTH & DESIGN

pubs.acs.org/crystal

Review

Progress in Energy–Safety Balanced Cocrystallization of Four Commercially Attractive Nitramines

Published as part of Crystal Growth & Design special issue "Honoring Professor Jagadese J. Vittal and his Contributions to Functional Molecular Crystals".

Veerabhadragouda B. Patil* and Svatopluk Zeman

Cite This: *Cryst. Growth Des.* 2024, 24, 7361–7388

Read Online

ACCESS | Metrics & More | Article Recommendations

ABSTRACT: In 2011, cocrystallization of energetic materials became a hot topic and a pathway to overcome the energy–safety contradiction; especially for commercially attractive nitramines, it became the first preference for researchers. The present review focuses on the energetic–energetic cocrystallization of four commercially attractive nitramines, CL20, HMX, BCHMX, and RDX, the structural aspects of these cocrystals, and their influence on thermochemical and detonation properties. Cocrystallization has proven to be a crystal engineering technique to achieve the safety and morphological suitability of energetic–energetic cocrystals (EECCs). Overall, in most of the cases, the impact sensitivities of EECCs are decreased, and this is a phenomenal change; however, it needed to adjust with detonation properties slightly, and it is negligible if the coformer energetic materials (EMs) are properly chosen. There are other notable variations in the crystal morphologies and packing of crystals, including key properties such as relatively high density and melting point. These changes occur due to the binding energy, trigger bond energy, trigger bond length, and cohesive energy density of EECCs during cocrystallization. Researchers highly focused on cocrystallization of these four nitramines; earlier reported methods are lacking in selectivity and scalability. When it comes to adoption to industrial scale production of EECCs, it is more difficult. We conducted a thorough literature survey. Also we discussed about a recently developed VPSZ coagglomeration method, which provides a huge opportunity to tune the key properties and performance of existing energetic materials and is easy to scale up to the industrial level.

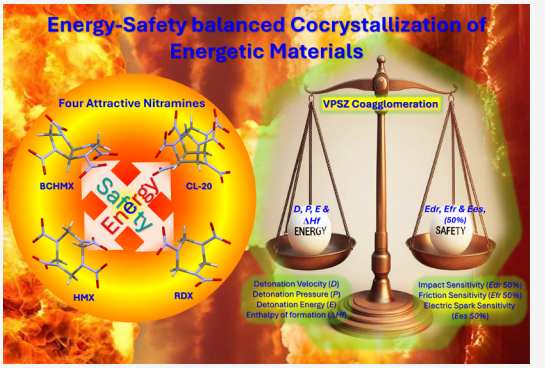

1. INTRODUCTION

1.1. Research Background. Energetic materials (EMs: explosives, propellants, and pyrotechnics) are widely used for military as well as civil applications.[1] Despite their production and handling risks, these materials have proven indispensable in military and civilian uses. Evolution has been slow for over 1200 years; black powder prevailed until the early 20th century. Researchers synthesized various EMs based on the requirements; however, synthetic methods have gradually reached saturation. More attractive energetic materials inherit the problem of impact sensitivity. To overcome this property, several efforts have been made by researchers to achieve energy–safety balanced EMs. Several methods emerged, like improved crystallization, coating with insensitive materials to modify surface morphology and shape of the crystals,[2] mixing with energetic or nonenergetic materials, polymer coating,[3] cocrystallization, etc. (Figures 1 and 2).

These efforts continued; however, approaches have been focused along with sensitivity on key research components, viz., thermal stability and detonation properties of EMs.[4] Later, cocrystallization with energetic–energetic materials began to emerge. Initially, it did not grab the attention of researchers significantly, but from 2010 onward, it became a hot topic for researchers from both scientific and technological points of view. This review attempts to focus on recent developments in a compatible and easily scalable approach with attainable high-purity, i.e., coprecipitation followed by coagglomeration.

This review can be a reference for exploring high-performance cocrystals of energetic materials in a scalable approach for future applications and specific activities for space and military purposes,[5] which need to be explored.

Received: May 21, 2024
Revised: July 30, 2024
Accepted: July 31, 2024
Published: August 19, 2024

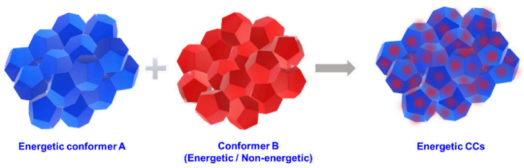

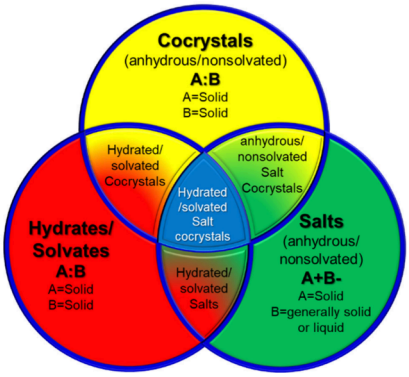

Figure 1. (a) Schematic of cocrystals (CCs) of energetic materials; if coformer B is energetic they are known as energetic−energetic cocrystals (EECCs). (b) Multicomponent solid forms inherently overlap with one another and in addition they can exhibit polymorphism. Recreated from ref 6. Copyright 2012 American Chemical Society.

1.2. Research and Developments in Cocrystallization of Energetic Materials. Cocrystallization is more attractive to researchers as an alternative route in development of the novel properties with existing energetic materials rather than synthesizing new materials[7,8] (Figure 1). This method also helps to alter the physiochemical properties as well as performance and strengthen the safety of the EMs.[7] It is a most promising method to develop excellent energetic materials, as it can achieve a favorable balance between high energy and low sensitivity for the energetic materials by tuning their components and ratios.[4,7,8]

Considering these aspects, much research and development has been happening in cocrystallization of EMs, not only in preparations but also in simulation to understand the intermolecular structural orientations and compatibility.[8−10] Cocrystallization of EMs can be performed mainly in two ways: one with nonenergetic materials and another with energetic molecules (the second approach is addressed mainly in this review article). If a single crystal is grown successfully, the characterization will be easier; otherwise it is a bit challenging.[11] There are different methods of preparation (discussed in section 2) which vary with thermochemical and instrumental conditions.[12]

2. PREPARATION METHODS AND TECHNIQUES

2.1. Evaporation Crystallization. Evaporation is the most commonly used method in cocrystallization, mainly used for development or to grow single crystals of cocrystals (Figure 3 and Table 1). In this method, complete crystallization is achieved via allowing solvent to slowly evaporate. Selection of solvents is challenging in this method because both coformers may have great differences in solubility.[13] Crystal free-growth shapes are not controllable in this method and yielded single crystals are more beneficial to scientific studies than technological applications; that is, sometimes crystals appeared to be sharp needles that possess mechanical sensitivity that will be retained or increased (Table 1).[7,12,14] In addition to this, sometimes solvate might form with usage of large amounts of solvent, long time, and development of larger crystals, which might cause low yield, irregular shape and size, etc. of cocrystals.[12]

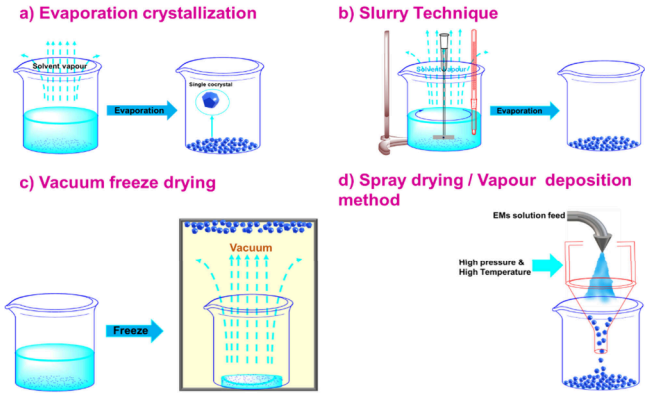

Figure 3. Schematic representation of different cocrystallization methods.

However, complementary procedures have been developed to improve this method, especially rapid evaporation; yet the aforementioned problems cannot be completely avoided, especially when there is a likelihood of solvate formation,

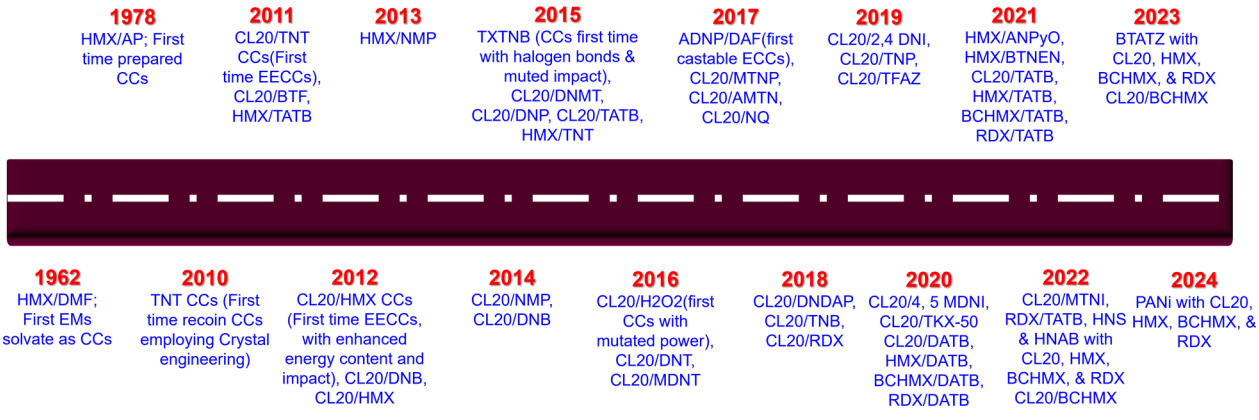

Figure 2. Schematic roadmap: evaluation of cocrystals in attractive nitramines.

https://doi.org/10.1021/acs.cgd.4c00686
Cryst. Growth Des. 2024, 24, 7361−7388

Table 1. EECCs of Attractive Nitramines Using Evaporation Method

cocrystal (A/B)	solvent system	particle size	shape	ref
CL20/TNT	EtOH	<500 μm	hexahedral cubicles	15
CL20/BTF	EtOH	*a*	hexagonal elongated	16
CL20/TNT	EtAc/DMK/Toluene/CH_2Cl_2	>100 μm	*a*	17
CL20/DNB	EtOH	>100 μm	block prism	18
CL20/MTNP	EtAc	>100 μm	irregular blocks	19
CL20/RDX	ACN	>50 μm	rod like	20
CL20/AMTN	EtOH/EtAc	>100 μm	*a*	21
CL20/2,4-MDNI	EtOH	>100 μm	hexahedral prism	22
CL20/4,5-MDNI	EtOH	>100 μm	broken rod like	
CL20/MTNP	EtOH	500 μm	flattened square	23
CL20/HMX	DMK; DMK+H_2O	20−100 μm	irregular	24
CL20/1,4-DNI	EtAc	>100 μm	rod like	25
CL20/TNP	EtAc/DMK/CAN	*a*	*a*	26
CL20/pyrazine	EtAc	>100 μm	*a*	27
CL20/pyrazine	MeOH+EtAc	>100 μm	*a*	
CL20/4,5-MDNI	ACN	>100 μm	square cubes	28
CL20/4,5-MDNI	EtOH	>100 μm	elongated cubes	
CL20/TFAZ	H_2O	1 mm	chunk-like	29
CL20/MTNI	MeOH	>100 μm	irregular	30
CL20/BTF	EtOH	>100 μm	*a*	31
DNP/DAF	H_2O	>100 μm	needle	32
DNP/DAF	H_2O + 30% H_2O_2	>100 μm	square	32

[a]Not applicable.

Table 2. EECCs of Attractive Nitramines Using Spray Drying Method

cocrystal (A/B)	solvent system	particle size	shape	ref
HMX/AP	DMSO	30−300 μm	*a*	36
n-K6/n-RDX	DMK	82 nm	hexagonal flat	37
Keto-RDX (2-oxo-1,3,5-trinitro-1,3,5-triazacyclohexane, K6)				
HMX/TNT	DMK	50−200 nm	spherical	38
CL20/HMX	DMK	50−100 nm	spherical	39
CL20/HMX	DMK	100 mm		
CL20/HMX	DMK	100 mm	spherical	40
CL20/HMX + PVAc	DMK	100−1000 nm	spherical	41
CL20/DNDAP	MeAc	0.5−5 μm	spherical	42
CL20/TNT	EtAc	200 nm	irregular	35
CL20/DNB	BuOn	100−500 nm	irregular	35
CL20/TNB	*n*-BuAc	200−600 nm	irregular	35
CL20/2,4-DNI	DMK	518.25 nm	spherical beads	34
CL20/NQ	DMSO	>50 μm	spherical	43
CL20/HMX/DOS	ACN	±1 μm	hollow networked flakes	44
CL20/HMX/PVAc				
CL20/HMX/PVB				

[a]Not applicable.

difficult separation, and low yields, creating uncertainty in the feasibility of producing CCs of EMs due to the different shapes of EECCs (Table 1).

2.2. Spray Drying/Vapor Deposition Technique. In this technique, coformer EMs are dissolved selective solvents and then dried into a powder form by spraying the liquid feed into a hot drying medium[33] (Figure 3). Recently, this technique is getting more attention from researchers to obtain nanosized cocrystals with an equimolar distribution of crystals. This process is quicker and easier for obtaining nanosized crystals; more details of the obtained crystal morphological properties are shown in Table 2. However, the safety of the preparation of cocrystals is decreased at large-scale. This process is not very compatible with certainty due to the possibility of formation of flakes if crystals are not dried completely (aspects of their sensitivity), which are not usable in ammunitions. Also, difficulty in designing the spray nozzle, pressure maintenance, and sometimes different masses of small droplets cannot be completely mitigated due to the uniform direction of draft and gravity, resulting in agglomeration when not completely dried. However, there are efforts to scale up this process due to it being a one step process and faster and providing greater continuity[34,35] (as shown in Table 2).

2.3. Slurry Technique. This technique is usually a solvent mediated one; both coformers are dissolved in a solution, and controlled evaporation of the solvent is induced (Figure 3). Slurry forms at the initial stage; later, dried cocrystals are obtained, which are controlled in size and shape by means of the stirring process and solvent addition variation. This method is easily adaptable to larger-scale production compatible with scale-up. In this method, both coformers undergo good reaction with each other in a solvent medium with controlled size growth of the crystals. The risk of adulteration with external materials is low, as the technique involves continuous mixing and the obtained cocrystals also show structural homogeneity[45] (as shown in Table 3). So, it is also generally known as reaction cocrystallization, and it has been extensively used as an efficient, straightforward cocrystallization screening method. However, only a few attempts at utilizing this method for scaled-up cocrystal production have been undertaken, and none have realized its full potential by utilizing solid dosing and a process of analytical technology. Semibatch reaction cocrystallization (SBRC) provided the first scale-up for high quality CL20/HMX cocrystals (Table 3).

2.4. Vacuum Freeze-Drying. In this process, a solution of EMs in a completely frozen form is placed under a vacuum in order to remove the solvents, allowing the solvents to change directly from solid to vapor without passing through a liquid phase, also known as sublimation drying (Figure 3). In this method, the solution is frozen quickly so that the cocrystal growth and aggregation process is very short, which is helpful to form the nanosized cocrystals.[12,43]

This method, slightly modified by eliminating the freezing condition, is known as vacuum pyrolysis. Basically antisolvent extraction from the cocrystal solution is applied to remove the solvent molecules from the solvates.[64] In both methods, the basic difference is vacuum drying is based on the boiling point of water, and vacuum freeze-drying is based on the melting point of

https://doi.org/10.1021/acs.cgd.4c00686
Cryst. Growth Des. 2024, 24, 7361−7388

Table 3. EECCs of Attractive Nitramines Using Slurry Method

cocrystal (A/B)	method used	solvent system	particle size	shape	ref
HMX/TATB	SLM co-precipitation	DMSO/H_2O	20−30 μm	prismatic type microstructure without apparent crystal edges	46
CL20/TNT, CL20/HMX	SLM & EVM	various organic solvents	100 μM	hexagonal prismatic	47
CL20/HMX	SLM & EVM	acetone & acetone/propanol	>100 μM	irregular square & pentagon	48
CL20/TNT	SLM co-precipitation	EtAc + dextrin/H_2O	100 μM	prism shaped with slightly smoothed edges	38
CL20/DNMT	SLM resonant acoustic mixing process	ACN	NA	hexagonal	49
CL20/TATB	SLM co-precipitation	DMSO	>3−5 μm	hexagonal irregular bulk crystals	50
CL20/HMX	SLM bead milling	H_2O/PVA	<200 nm	square cubes	51
CL20/MDNT	SLM solvent agitation	ACN	>100 μm	*a*	52
CL20/RDX	SLM ball milling	EtOH/H_2O	123.8 nm	spherical	53
CL20/TNT	SLM ball milling	EtOH	100 μm	regular hexahedral	54
CL20/HMX	SLM resonant acoustic mixing process	DMK/xylene/dextrine	101 μm	diamond	55
CL20/TNT	SLM ball milling	EtOH	119.5 nm	irregular spherical	56
HMX/ANPyO	SLM co-precipitation	DMSO/glyoxal/H_2O	50−150 μm	irregular polyhedron	57
HMX/ANPyO	SLM co-precipitation	DMSO/glyoxal/H_2O	50−150 μm	irregular polyhedron	57
HMX/BTNEN	SLM co-precipitation	DMK/CH_2Cl_2/hexane	*a*	broken crystal	58
CL20/HMX	SLM reaction crystallization	ACN	0.02 cm	cubic	59
CL20/HMX	SLM co-precipitation	DMSO/H_2O	21.8 μm	cubic	60
RDX/TATB	SLM co-precipitation	distilled water	30−40 μm	granules	61
CL20/MTNP	solvent agitation	EtOH/IPA	>100 μm	linear	62
HMX/NTO	co-precipitation	H2O	>100 μm	granules	63

[a]Not applicable; SLM, slurry method; and EVM, evaporation method

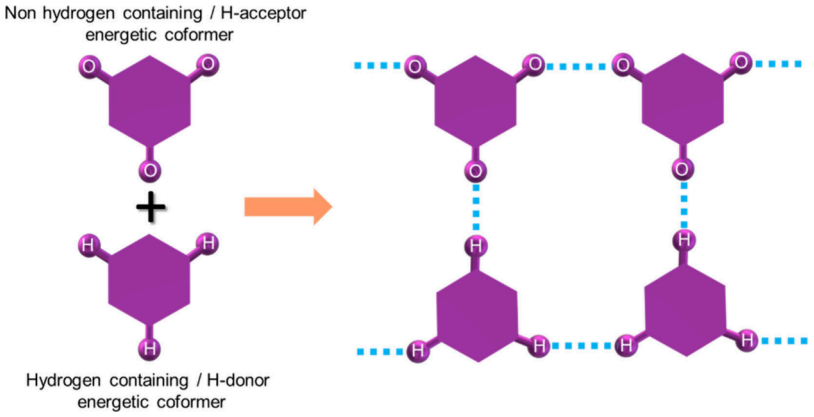

Figure 4. Schematic of coformer interactions in crystalline lattice: one hydrogen containing energetic coformer acts as hydrogen donor and a nonhydrogen containing energetic coformer acts as hydrogen acceptor with hydrogen bonding and intermolecular interactions (as shown in Figure 5B) between both coformers forming EECCs.[71]

water. Moreover, this method needs to maintain a continuous high vacuum; otherwise, cocrystallization ends with a slurry and wet crystals.

3. COMPONENTS SHAPING COCRYSTALS: INTERMOLECULAR INTERACTIONS

Usually, the individual coformers exhibit hydrogen bonds between them to form a stabilized crystal lattice. Several researchers found that in cocrystals, the coformers are connected by attractive intermolecular/interlayer electrostatic interactions.[8,65]

These interactions also help to stabilize both coformers in the single crystal lattice, i.e., in the cocrystal form. According to the component and structural types of the entities involved in the interactions, intermolecular interactions (noncovalent interactions) are divided into van der Waals interactions (dispersion interactions) and electrostatic interactions (Coulomb interactions). Chemically, they can also be referred to as hydrogen bonding (HB), halogen bonding, or stacking.[5,8,66]

3.1. Hydrogen Bonding. When a molecule can act as a hydrogen bond donor, the hydrogen or hydrogens under examination are characterized by relatively strongly positive molecular surface electrostatic potentials. In general, hydrogen bonding involves a donor and an acceptor containing an acidic hydrogen atom and an electronegative atom (N, O, F, etc.), respectively[65,67] (Figures 4 and 5B). Hydrogen bonding consequently tends to be less directional than halogen bonding and other σ-hole interactions.[68] Hydrogen bonds can be classified based on their bond energy as weak, moderate, and strong.[69] However, energetic molecules are usually short of active hydrogen atoms and cannot form strong hydrogen bonds[68] (see Figures 4 and 5). In the case of the polynitro

https://doi.org/10.1021/acs.cgd.4c00686
Cryst. Growth Des. 2024, 24, 7361−7388

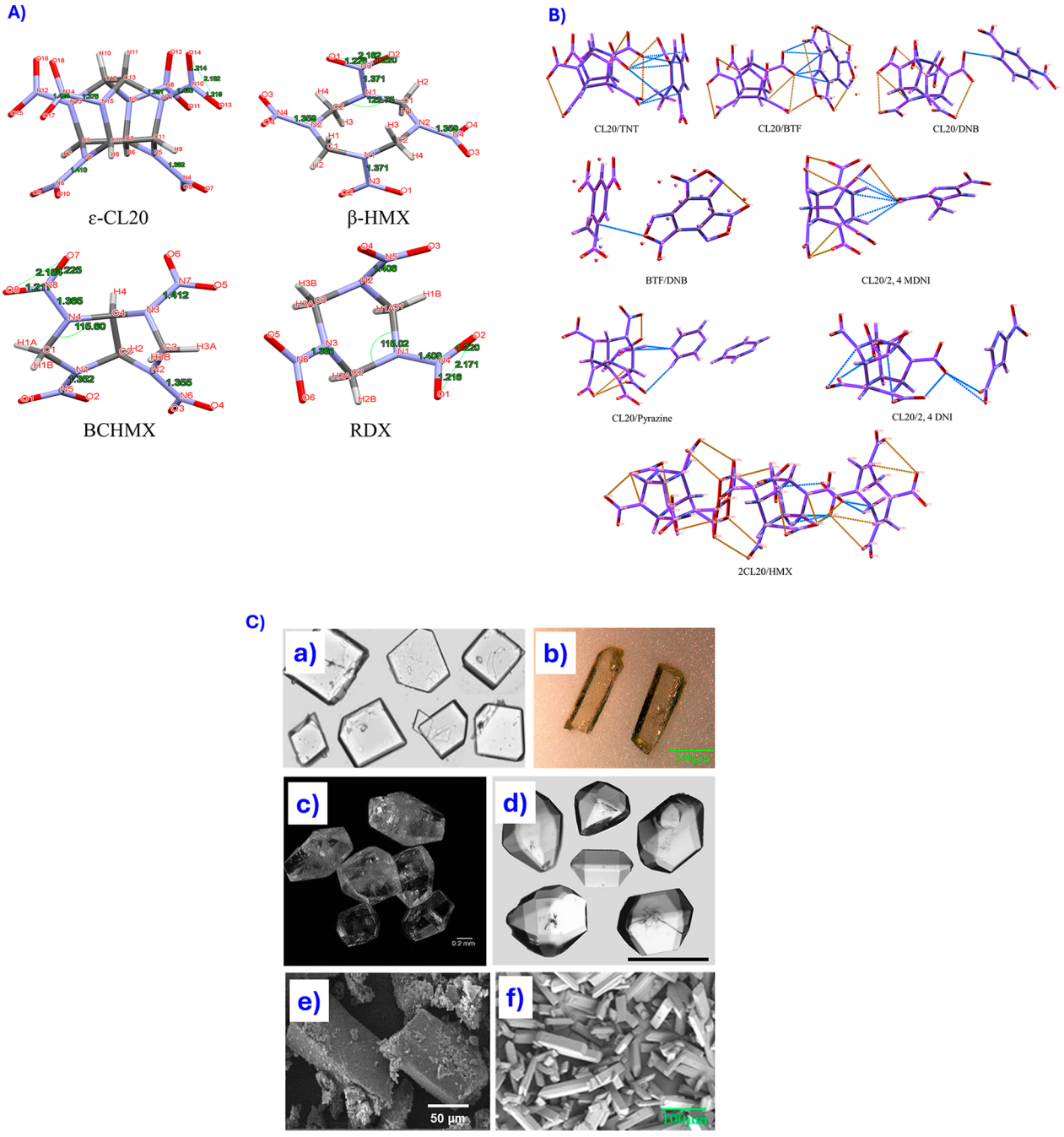

Figure 5. (A) 3D Single crystal XRD molecular structures of four attractive nitramines with internal atomic distances. *ε*-CL20 reproduced with permission from ref 83. Copyright 2004 International Union of Crystallography. *β*-HMX reproduced with permission from ref 84. Copyright 2020 American Chemical Society. BCHMX reproduced with permission from ref 85. Copyright 2009 Elsevier. RDX reproduced with permission from ref 86. Copyright 2008 International Union of Crystallography. (B) 3D Single crystal XRD molecular structures of EECCs of nitramines; here, orange colored bonds indicate pure hydrogen bonds, whereas blue colored bonds indicate electrostatic intermolecular short contacts developed between both coformers during cocrystallization. CL20/TNT reproduced with permission from ref 15. Copyright 2011 John Wiley and Sons. CL20/BTF reproduced with permission from ref 16. Copyright 2012 American Chemical Society. CL20/DNB reproduced with permission from ref 18. Copyright 2014 John Wiley and Sons. BTF/DNB reproduced with permission from ref 87. Copyright 2014 John Wiley and Sons. CL20/2,4-MDNI reproduced with permission from ref 22. Copyright 2018 American Chemical Society. CL20/pyrazine reproduced with permission from ref 27. Copyright 2019 American Chemical Society. CL20/2,4-DNI reproduced with permission from ref 25. Copyright 2019 American Chemical Society. 2CL20/HMX reproduced with permission from ref 48. Copyright 2012 American Chemical Society. (C) SEM images of the cocrystals: (a) CL20/HMX reproduced with permission from ref 48. Copyright 2012 American Chemical Society. (b) CL20/BTF reproduced with permission from ref 16. Copyright 2012 American Chemical Society. (c) CL20/DNB reproduced with permission from ref 18. Copyright 2014 John Wiley and Sons. (d) CL20/TNT reproduced with permission from ref 15. Copyright 2011 John Wiley and Sons. (e) BTEN/HMX reproduced with permission from ref 58. Copyright 2020 John Wiley and Sons. (f) CL20/1,4-DNI reproduced with permission from ref 25. Copyright 2019 American Chemical Society.

compounds studied here, the donor hydrogen tends to approach the nitro-O atoms in the C-NO_2 (N-NO_2) plane and in an approximate 3:2 ratio, which occurs between the two nitro-O atoms rather than between the C and the O substituents (if

https://doi.org/10.1021/acs.cgd.4c00686
Cryst. Growth Des. 2024, 24, 7361−7388

present). However, the hydrogen approach between the two O acceptors is usually strongly asymmetric, with the H atom more closely bonded to only one of the O atoms.[70]

Generally, strong hydrogen bonds are shorter, which strongly influences the formation of a stable cocrystal.[72] This is not only true in cocrystals, for example, the complete nitration of the polyamino-arenes to the polynitro derivative as in 1,3,5-triamino-2,4,6-trinitrobenzene (TATB) increases its chemical stability with formation of short intra- and intermolecular H-bonding[73] (see Figure 6). Hydrogen bonds also have an obvious

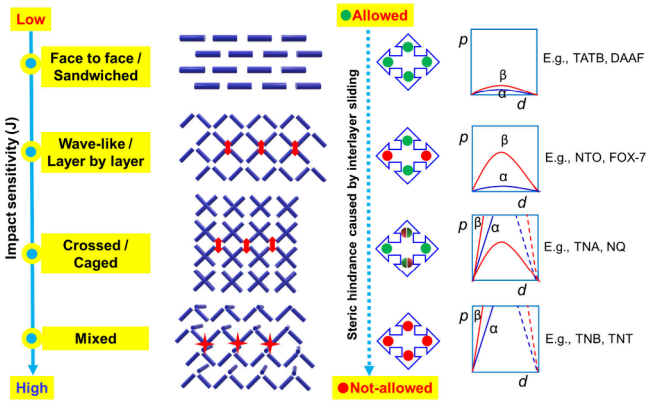

Figure 6. Schematic of the principle of crystal packing−impact sensitivity relationship by π-stacked energetic crystals with a few suitable examples. In the third column, the four arrows symbolize interlayer sliding directions (right/left and up/down) with interlayer sliding allowed (in green), not allowed (in red), and partially allowed (in red/green) for the four kinds stacking. The plots show packing modes and inter/intramolecular potential (p)−sliding distance (d) dependencies of four kinds of stacking. α and β denote sliding along left/right and back/front directions, respectively. Recreated from refs 94 and 95. Copyright 2014 and 2020 American Chemical Society.

effect on trigger bond lengths when the molecule undergoes cocrystallization for a nitramine like HMX with MDNI.[74] In the case of a crowded molecule like CL20 undergoing cocrystallization with TNT, HMX, RDX, FOX-7, MDNT, or TEX, primarily, H-bond formation takes place between -NO_2 and hydrogen atoms via H···O or H···N bonds[10,75−77] (see Figures 5A,B and 6). However, H-bonding interactions which are bonded to carbon atoms are not referred to as hydrogen bonds; these interactions are the result of molecular packing[16] (which is discussed in detail section 3.4).

3.2. π-Stacking ($\pi-\pi$ and n$-\pi$). Intermolecular stacking between the two coformers is denoted as π-stacking; if this interaction is a lone pair of one coformer with the π-structure of another, it is referred to as n$-\pi$ stacking, and similarly, if both interacting parts have π structure, it is denoted as $\pi-\pi$ stacking. This stacking possesses a donor−acceptor couple of both coformers. $\pi-\pi$ stacking is stronger and well-studied, whereas n$-\pi$ stacking is weaker and still needs to be studied actively; usually it occurs in crystals of stacked planar molecules with strong hydrogen donors and acceptors.[5,66,78] These stacking changes actively influence intermolecular arrangement and respond to stimuli via converting mechanical to intermolecular interaction energy, which disperses throughout the stacked layers of the EECCs; in ascending order the interactions are wavelike (layer-by-layer), crossed (caged), face-to-face (sandwich), and mixed stackings[79,80] (see Figure 6). These π-stacking interactions between -NO_2 groups and aromatic rings form herringbone-like structures via stacking groups.[81] Even though PETN, RDX, HMX, and CL20 lack conjugated frames, their molecular stacking patterns can still be directly described using the stacking patterns of molecules that are in closer contact with one another.[82]

3.3. van der Waals Interactions. van der Waals forces are a kind of intermolecular interaction that is very different from the hydrogen bonds, which are composed of polarization and charge transfer effects.[88,89] Normally, the distances of intermolecular forces (van der Waals interactions and hydrogen bonds) are in the range of 3.10−5.03 Å and 1.10−3.10 Å.[90] These interaction forces enhance bond lengths of the N−NO_2 bond in EECCs with aromatic coformers like DNT[91] (see Figure 5B). Also, this interaction forces a weaker frozen effect for coformers in EECCs (ΔE_{frozen}).[92] Along with HBs, these interactions play a key role in improving the density of the EECCs.

van der Waals and weak steric intermolecular interactions may be the primary causes of the formation of CL20/MTNP cocrystals, as a typical example with high density. However, hydrogen bonds are the strongest intermolecular interactions, and all others are much weaker. All have a significant impact on the final physical properties.[12]

3.4. Packing of Structures: Layered Stacking, Channel Stacking, and Caged Stacking. Packing of structures plays an important role in defining the sensitivity and performance of EECCs. The detonation properties, sensitivity, and other parameters of EMs are essentially determined by the packing configuration.[93]

First, we concentrate on the packing arrangements in CL20-based EECCs as examples, which have the same CL20 component but various coformers.[82,92] The strongest of these three intermolecular interactions, HBs, strengthens crystal packing by enhancing interactions between component molecules, while stacking, especially face-to-face stacking, tends to reduce the mechanical sensitivity of energetic crystals (see Figure 6). Halogen bonding is thought to be rare, but it can potentially alter the molecular stacking structure through cocrystallization.[8]

Layered packing is less sensitive;[96] however, for sheet-like or herringbone lattice structures, they are more sensitive similarly if their zigzag packing makes a more stable crystal lattice.[93,94] A thorough examination using single crystal X-ray diffraction to analyze structural variables revealed the significance of weak interactions, particularly interactions and hydrogen bonds in close packing.[67] It should be noted that packing efficiency, which may be confirmed by an analysis of packing coefficients, also adds to an EM's high density, e.g., ε-CL20/TNT.[5,90,97] These are key intermolecular aspects of cocrystals briefly covered here that play an important role in crystal engineering; instead of creating new molecules with the desired properties, packing structures and physicochemical properties can be changed by manipulating existing molecules.[92,98]

4. THERMOCHEMICAL PROPERTIES OF COCRYSTALS

Thermal stability and sensitivity are the main concerns with regard to energetic materials, because inadequate thermal stabilities greatly restrict their application. A crucial factor in determining thermal behavior and assessing the potential of energetic materials for real-world use is thermal analysis.[99] The cocrystals have exceptional thermal stability and a rapid rate of energy release, according to thermal studies and calculations of detonation characteristics.[50] The EECCs' crystal packing and their lattice energy cause significant changes in thermal

https://doi.org/10.1021/acs.cgd.4c00686
Cryst. Growth Des. 2024, 24, 7361−7388

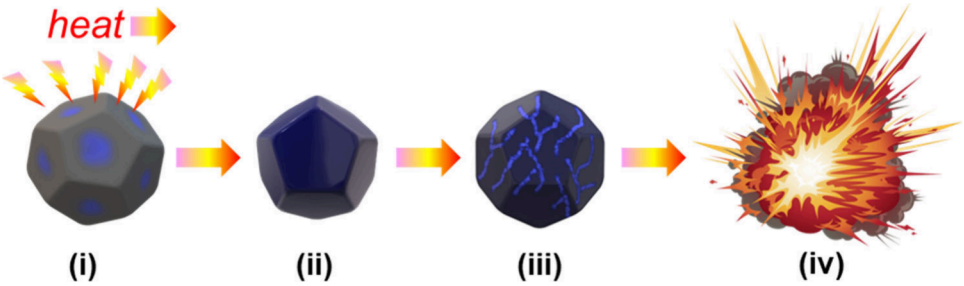

Figure 7. Schematic of thermal behavior of the CCs: (i) heating of the nitramine; heat supply surrounds the surface of the cocrystal; (ii) heat absorbed causes polymorphic change in nitramine crystal and coformer intermediate conversion; (iii) cracking of the nitramine crystal (for HMX, BCHMX, and CL20 see ref 17); (iv) spontaneous decomposition and/or explosion.[106]

behavior.[100] Therefore, based on the observed thermal data, they are differentiable as a physical mixture, and no clear differences in thermal stability were attributable to cocrystallization.[101] At the same time, there is significant inconsistency between impact sensitivity and thermal stability, and high thermal stability does not necessarily imply low impact sensitivity.[5]

4.1. Decomposition Temperature. Continuing activity on thermal stability is needed to focus on the decomposition temperatures of EECCs and compare them with the pure coformer EMs. It is also necessary to adopt new storage and transport conditions to avoid the self-accelerating decomposition temperature (SADT).[102] Usually, CCs exhibit decomposition at slightly lower temperatures than pure coformers do.[30] In some cases, a slight increase in decomposition temperature also takes place[103] (see Figure 7). Overall, for the majority of cases, cocrystallization alters physicochemical behavior, including melting and decomposition temperatures (5−10 °C) based on intermolecular interactions and crystal packing[55] (as shown in Table 4). This happens because the initial reactive products of coformer A further react with coformer B. Heat will be carried forward and come in contact with high temperature before leaving the crystal surface it causes initiation, e.g., CL20/HMX.[55] However, cocrystals can withstand the initial endothermic changes to a certain extent. Further detailed study of thermal behavior at different heating rates of EECCs found that decomposition temperature is directly dependent on heating rate[31,104,105] (see Figure 7).

The volume of decomposition products grows as the temperature rises during the thermal breakdown process, but the time to equilibrium and the potential energy decrease.[107] Although the decomposition temperature is modified to a certain extent, selective coformers for cocrystallization with TATB are a type of explosive that is thermally stable and insensitive, e.g., HMX/TATB.[103]

4.2. Heat of Combustion and Enthalpy of Formation (ΔH_{form}). In order to evaluate the performance of the EECCs as part of the application, Q_c and ΔH_{form} are usually calculated by using Hess law.[108] Enthalpy of formation (ΔH_{form}) needs to be calculated on the basis of the heat of combustion measurements,[109] and on the basis of obtained data, it is possible to calculate thermochemical and detonation parameters using CHEETAH, Explo5, and RoseBoom codes[110−112] (See Table 5 and Table 7). However, researchers are more focused on scientific work in EECCs, but a technological orientation is also needed.

Heat release rate is important for the combustion and mainly the detonation performance of these EECCs, which are also dependent on the stoichiometric ratio of coformers and the reaction conditions.[57,120] The enthalpy of formation, ΔH_{form}, indicates the energetic content EECCs; higher heat of combustion corresponds to lower energetic content, and the ΔH_{form} values with oxygen balance affect the heat of detonation.[14,121] It also follows, as has been confirmed, that there is a direct very good linear relationship between the heat of combustion and the experimental relative explosive strength of EMs.[122] Inert heating, thermal decomposition (or the beginning of gasification), main flame occurrence, secondary flame development, "snap-back", and establishment of steady-state combustion are all terms used to characterize the ignition process.[123]

Combustion also depends on the morphology of crystals, with porous RDX showing improved combustion properties.[64] Transition metals are commonly used as combustion catalysts; these compounds increase the efficiency of EM energy release.[12] Since increasing heterocyclic rings in molecules can significantly increase the enthalpy of formation, assembling various nitrogen-rich heterocycles like pyrazole units is a proven method in this area, as shown in ref 124. Recent research has looked into how the thermal decomposition and combustion behavior of cocrystals are impacted by nonbonding interactions, e.g., with CL20/HMX.[55] All these aspects are helpful to build the groundwork for industrial applications of EECCs by investigating their ignition and combustion mechanisms.[12]

4.3. Crystal Density. The most significant advances in energy density in the past 100 years have been achieved largely by increasing the physical crystal density of HEDMs by the use of more efficiently packed crystals with high crystal density[125] (Table 5). However, excessive H atoms are disadvantageous to increase energy density because covalent H atoms usually have a lower mass density than O and N atoms, leading to a lower crystal packing density.[71] The density of the cocrystals prepared exceeds 99% of the theoretical maximum density of the starting nitramines.[108] The detonation velocity of explosives is proportional to the density, and thus the crystal packing of energetic materials[126] and, in some cases, cocrystallization enhances density, e.g., HMX/NTO[127] and BTF with different coformers.[128] Morphologically, EECC enhancement of crystal density indicates a decrease in explosive volume and the number of cavities or defects, which helps to increase detonation pressure.[45,54,129] Further, on the other side the stacking conditions in the crystal lattice of EECCs significantly contributes to it,[89] and the density gained by these intermolecular interactions is defined as cohesive energy density (CED).[130] Also, crystals with $\pi-\pi$ interactions showed good impact sensitivity with high energy density content, e.g., CL20/TNT and other EECCs with CL20.[90,107] Generally, nitrogen-rich EECCs have compact packing with strong binding strengths

https://doi.org/10.1021/acs.cgd.4c00686
Cryst. Growth Des. 2024, 24, 7361−7388

Table 4. Decomposition Temperatures EECCs of Attractive Nitramines

cocrystal	decomposition temp (°C)	technique used	ref
CL20/TNT	150	DSC	15
HMX/TATB	284.9	DSC	46
CL20/BTF	235	DSC-TG	16
CL20/HMX	240	DSC/hot stage microscope	113
CL20/TNT	212	TGA-DSC	17
CL20/DNB	242	DSC-TG	18
CL20/DNMT	*a*	DSC	49
HMX/TATB	231.8	DSC-TG	50
n-K6/n-RDX	234	DSC	37
HMX/TNT	290	DSC	38
CL20/MDNT	*a*	DSC	52
CL20/HMX	246.8	DSC	40
CL20/NQ	229.3, 257.4	DSC	43
CL20/MTNP	222	DSC	19
CL20/RDX	264.4, 285.8	DSC	20
CL20/RDX	227	DSC	53
CL20/2,4-MDNI	220	DSC	22
CL20/4,5-MDNI	220	DSC	22
CL20/HMX	248	DSC	55
CL20/DNDAP	214.2, 243.7	DSC	42
CL20/DNDAP	223.5, 254.1	DSC	
CL20/TNP	230.1	DSC	26
RDX/TMS	244	TGA-DSC	64
RDX/HMPT	243.7	TGA-DSC	
CL20/4,5-MDNI	219	DSC	114
CL20/4,5-MDNI	222	DSC	
HMX/ANPyO	284.1	DSC	57
HMX/ANPyO	284.1	DSC	57
HMX/BTNEN	*a*	DSC	58
CL20/HMX	245.4	DSC	60
CL20/BTF	224.1	DSC	31
DNP/DAF	211.5	TGA-DSC	32
RDX/TATB	244	DSC	61
CL20/MTNP	133	TGA-DSC	62
HMX/NTO composite	223.75	TGA-DSC	63
NBA/AmTz, NBA/TATOT, NBA/NPTA, NBA/DAG	222, 239, 232, 310	TGA-DSC	115
CL20/HMX/DOS	240	DSC	44
CL20/HMX/PVAc	242	DSC	
CL20/HMX/PVB	235	DSC	
TT/HNT	178	DSC	116
TT/HDNT	251	DSC	
TT/TNP	218	DSC	
HNTO/AN	*a*	*a*	117
TNB/1,4-DNI	84.4	DSC	118
TNB/DNMT	88.5	DSC	
CL20/HMX/MF	246.5−250.8	*a*	119

[a]Not applicable.

and packing coefficients, which give them high density and energy content.[97] However, cocrystals do not always have a higher density than their pure coformers; as said before, it also depends on crystal defects and morphology.[131] Overall compared with pure EMs, EECCs have shown improved physiochemical properties such as solubility, stability, and density[132] (Table 5).

Table 5. Thermochemical Properties of EECCs of Attractive Nitramines

explosive				
code designation	molar ratio	ΔH_f (kJ mol^{-1})	crystal density (g·cm^{-3})	ref
CL20/TNT	1:1	*b*	1.84−1.91	15
CL20/BTF	1:1	*b*	1.918	16
CL20/HMX	2:1	*b*	1.945	113
HMX/NMP	1:1	*b*	1.571	126
CL20/TNT	1:1	*b*	1.760	133
CL20/DNB	1:1	*b*	1.880	18
CL20/TNT	1:1	*b*	1.846	18
CL20/DNMT	1:1	*b*	1.920	49
HMX/TATB	8:1	*b*	1.960	50
n-K6/n-RDX	1:1, 1:2	*b*	*b*	37
HMX/TNT	2:1, 3:1	*b*	*b*	38
CL20/HMX	2:1	*b*	*b*	51
CL20/MDNT	1:1	2166	1.883	52
CL20/NQ	1:1	186.61, 468.91	*b*	43
CL20/MTNP	1:1	793.9	1.932	19
CL20/AMTN	1:1	*b*	1.710	21
CL20/RDX	1:1	202.33	*b*	53
CL20/2,4-MDNI	1:1	*b*	1.867	22
CL20/4,5-MDNI	1:1	*b*	1.882	22
CL20/TNT	1:1	*b*	1.934	54
CL20/HMX	2:1	*b*	1.961	55
CL20/DNDAP	2:1	732	1.871	42
CL20/2,4-DNI	1:1	−708	1.84−2.01	34
CL20/1,4-DNI	1:1	*b*	1.922	25
CL20/4,5-MDNI	1:3	*b*	1.813	114
CL20/4,5-MDNI	1:1	*b*	1.882	
HMX/ANPyO	4:1	582.4	1.940	57
HMX/ANPyO	8:1	582.4	1.920	57
HMX/BTNEN	2:1	*b*	1.930	58
CL20/TFAZ	1:1	1164.2	1.932	29
CL20/HMX	(0.482−0.916): (0.463−0.898)	*b*	1.954	59
CL20/HMX	3:1	*b*	1.955	60
NBA:AmTz, NBA:TATOT, NBA:NPTA, NBA:DAG	1:1, 1:2, 1:1, 1:1	*b*	1.80; 1.71; 1.74; 1.76	115
CL20/HMX/DOS	*a*			44
CL20/HMX/ PVAc	*a*	−505 ± 13	*b*	
CL20/HMX/PVB	*a*			
TT/HNT	1:1	*b*	1.492	116
TT/HDNT	2:1	*b*	1.403	
TT/TNP	1:1	*b*	1.703	
HNTO/AN	1:3	−505 ± 13	*b*	117
TNB/1,4-DNI	1:1	*b*	*b*	118
TNB/DNMT	1:1	*b*	*b*	
CL20/HMX/MF	2:1	*b*	1.88−1.93	119
CL20/MTNP	1:1	*b*	*b*	62
HMX/NTO composite	4.0:0.1	*b*	*b*	63
DNP/DAF	1:1	*b*	1.68	32
DNP/DAF	1:1	*b*	1.76	

[a]Each category has five different proportions. [b]Not applicable.

https://doi.org/10.1021/acs.cgd.4c00686
Cryst. Growth Des. 2024, 24, 7361−7388

5. MECHANICAL SENSITIVITY OF COCRYSTALS: REACTION TOWARD EXTERNAL STIMULI

The sensitivity of an energetic material is represented by the minimum amount of force (or energy) applied to or required for EMs to reach a 50/50 probability of detonation from the point of view of physics of explosion. These tests are key evaluations for the safe handling of EECCs. Four sensitivities are generally reported for each EM: impact sensitivity (IS), friction sensitivity (FS), electrostatic discharge (ESD), and sensitivity to shock wave (SSW); the determination of the last one needs a bigger amount of sample and relatively complicated equipment; therefore, it is not usually a part of the basic research in energetic materials.

Classification of EMs is based upon the sensitivity; those sensitive to external stimuli are primary explosives (IS $\leq$ 4 J; FS $\leq$ 10 N; ESD = 0.002−0.020 J), while relatively insensitive ones are secondary explosives (IS $\geq$ 4 J; FS $\geq$ 50 N; ESD $\geq$ 0.1 J). Cocrystallization has shown a significant effect in the alteration of these sensitivities. Zeman et al. thoroughly studied the initiation reactivity of EMs in both their pure state (mainly) and under environmental conditions which are also responsible for sensitizing EMs.[134]

From a molecular point of view, mechanical perturbation of intramolecular vibrations and intramolecular stretching due to initiation impulses (the latter giving rise to collective delocalized excitations or phonons) leads either to energy transfer of vibrations to phonons (vibrational relaxation) or energy transfer from the phonons to vibrations (multiphonon up pumping)[135] (Figure 8a). This disruption should occur under extreme pressures and temperatures. Still, there is evidence that the first fragmentations of energetic molecules in initiation occur at conditions already milder than those prevailing at the front of the detonation wave and partially already before this front.[134] It is well-known that the phonon is one of the most important elementary excitations in solid systems as a factor related to the thermal properties and chemical stability of energetic materials, i.e., to the lattice stability, thermal properties, vibrational spectra, and initiation mechanisms shown in Figure 8a.[136]

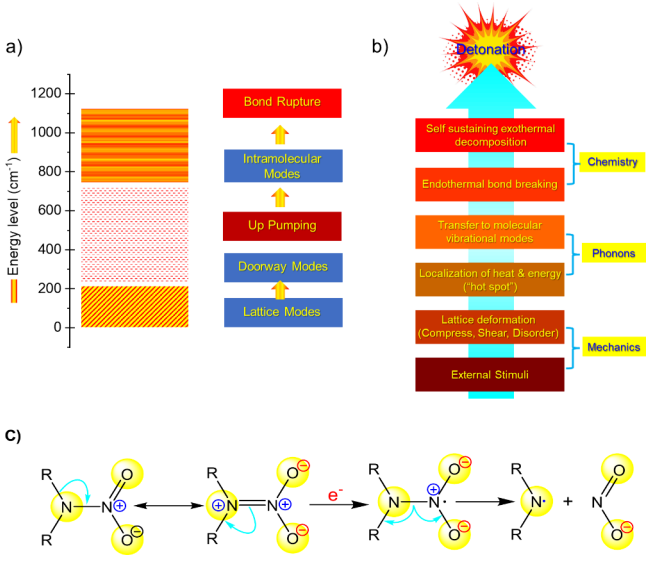

Figure 8. (a) Schematic diagram of the phonon up-pumping theory: external stimuli excite mechanical energy transfer into doorway modes and then doorway modes up-pump to intramolecular vibrations, which cause initiation. (b) Schematic diagram of shock-induced detonation mechanism of energetic crystals.[136] (c) Schematic diagram of electron attack on the nitramine group producing an aza-radical and a nitrite anion (the first step in the nitramine electro-reduction).[144]

The initiation of energetic materials by heat, impact, shock, friction, and electric spark should have a common mechanism of primary splitting of their molecules.[137] For the study of the listed types of EM initiation reactivity, the application of thermoanalytical methods is advantageous.[137] Thus, for cyclic nitramines and PBXs at their base, a logarithmic relationship between impact energies and the zero-order isothermal decomposition rate constant has been described, according to which in the vast majority of cases an increasing value of this constant corresponds to an increase in the impact resistance of the investigated explosives (this relation is waiting for interpretation).[134] Similarly, the relationships between the activation energies of the thermal decomposition of nitramines, on the one hand, and both the impact and friction sensitivities, on the other hand, are described.[137]

In cocrystallization, the sensitivity of EECCs depends on the coformer EMs selected to modify the targeted EMs, their molar ratio, and their intermolecular interactions (section 3), crystallization method (section 2), as well as the obtained EECC crystal morphology, and is discussed briefly in the following (Table 6).

5.1. Impact Sensitivity (IS). The impact sensitivity determination primarily depends on many factors, especially the method of measurement and human error. According to theoretical and synthetic chemists, due to these aspects, corresponding outputs are not easy to correlate quantitatively with lattice parameters.[131]

However, if the methodology for determining this sensitivity by majority of researchers followed the BAM method, which is predominant in the world,[138] then for pure energetic materials, there are logical semilogarithmic relationships of impact energies to the characteristics of the pure EM molecular structure, represented by the ^{13}C or ^{15}N NMR chemical shifts of the key atoms in the reaction center of the molecules.[137,139] In connection with the above, a linear relationship between the impact energy (impact sensitivity) and net charge of the most reactive nitro group of nitramines and polynitropolyphenylenes is also logically described.[134]

The important relationship of impact sensitivity is to performance (volumetric heat of explosive or detonation energy) or better to the energy content (enthalpy of formation or heat of combustion) of energetic materials. Licht's rule that high power is usually accompanied by increased sensitivity and that an insensitive explosive does not exhibit peak performance applies here (although there are numerous exceptions and also is should be stated that this result is not yet supported by theory).[140,141]

In terms of the theory of up-pumping[135] (Figure 1.9a), there is a good correlation between the phonon vibration coupling model and the experimental impact and shock sensitivity of various secondary explosives. The more complex and denser the vibrational spectrum of the material, the greater the probability of phonon coupling with the oscillator, the faster the transfer of energy from the phonon manifold to the intramolecular vibration mode, and the more sensitive the energetic material.[142]

Theoretically, shear contact with the surface of EECCs initiates thermal heat transfer detonation; however, practically, there is a significant difference between the thermal stability and impact sensitivity, viz., high thermal stability does not necessarily indicate low impact sensitivity. Both characteristics depend on

https://doi.org/10.1021/acs.cgd.4c00686
Cryst. Growth Des. 2024, 24, 7361−7388

Table 6. Sensitivities of EECCs of Attractive Nitramines

EECCs (A/B)	impact sensitivity (J)			friction sensitivity (%)			electric spark sensitivity			ref
	A	B	A/B	A	B	A/B	A	B	A/B	
CL20/TNT	13.54	*a*	28.52	*a*	*a*	*a*	*a*	*a*	*a*	15
HMX/TATB	100%	*a*	10%	*a*	*a*	*a*	*a*	*a*	*a*	46
CL20/TNT, CL20/HMX	*a*	*a*	*a*	*a*	*a*	*a*	*a*	*a*	*a*	47
CL20/HMX	1.42	*a*	2.67	*a*	*a*	*a*	*a*	*a*	*a*	113
CL20/TNT	13	103	30	100	0	58	*a*	*a*	*a*	133
CL20/DNB	*a*	*a*	9.212	*a*	*a*	*a*	*a*	*a*	*a*	18
CL20/TNT	*a*	*a*	6.86	*a*	*a*	*a*	*a*	*a*	*a*	18
CL20/DNMT	12.838	>49	12.495	72	252	120	20/20 @ 0.051 J	20/20 @ 0.025 J	20/20 @ 0.025 J	49
HMX/TATB	2.25	3	3	*a*	*a*	*a*	*a*	*a*	*a*	145
n-K6/n-RDX	<1.56	2.05	3.03	72	180	168	0.158	0.359	0.246	37
HMX/TNT	4.802	36.652	15.215	*a*	*a*	*a*	*a*	*a*	*a*	38
CL20/MDNT	19.6	5.1352	4.998	72	128	120	20/20 @ 0.05 J	20/20 @ 0.5 J	20/20 @ 0.025 J	52
CL20/HMX	3.209	4.802	11.588	100	84	64	*a*	*a*	*a*	40
CL20/HMX	*a*	*a*	>78.6	*a*	*a*	*a*	*a*	*a*	*a*	41
CL20/MTNP	4	24.5	6	94	240	180	272	253	276	19
CL20/RDX	13.6	49.8	29.4	100	80	80	*a*	*a*	*a*	20
CL20/AMTN	3.43	25.24	10.54	*a*	*a*	*a*	*a*	*a*	*a*	21
CL20/RDX	7.35	20.408	25.2	100	74	56	*a*	*a*	*a*	53
CL20/TNT	3.185	23.275	10535	100	49	38	*a*	*a*	*a*	54
CL20/HMX	5.488	9.8	9.4	84−90	190−200	300−330	*a*	*a*	*a*	55
CL20/DNDAP	2.55	17.052	5.88	100	8	48	*a*	*a*	*a*	42
CL20/TNT	4	15	7.5	*a*	*a*	*a*	*a*	*a*	*a*	35
CL20/DNB	4	39	9	*a*	*a*	*a*	*a*	*a*	*a*	35
CL20/TNB	4	14	8	*a*	*a*	*a*	*a*	*a*	*a*	35
CL20/2,4-DNI	9.099	>49.01	29.57	120	>360	>360	*a*	*a*	*a*	34
CL20/1,4-DNI	2.5	14	10	*a*	*a*	*a*	*a*	*a*	*a*	25
CL20/TNT	6.37	45.08	19.11	100	4	68	*a*	*a*	*a*	56
CL20/4,5-MDNI	2.5	34	16	*a*	*a*	*a*	*a*	*a*	*a*	114
CL20/4,5-MDNI	2.5	34	11	*a*	*a*	*a*	*a*	*a*	*a*	
HMX/ANPyO	4	24	8	*a*	*a*	*a*	*a*	*a*	*a*	57
HMX/ANPyO	4	24	10	*a*	*a*	*a*	*a*	*a*	*a*	57
CL20/TFAZ	2.548	16.464	8.232	100	4	38	*a*	*a*	*a*	29
CL20/HMX	10	*a*	>20	80	144	168	*a*	*a*	*a*	60
CL20/MTNI	4	13	10	95	360	360	*a*	*a*	*a*	30
RDX/TATB	6	*a*	17.5	*a*	*a*	216	*a*	*a*	*a*	61
NBA/AmTz, NBA/TATOT, NBA/NPTA, NBA/DAG	*a*	*a*	>40 (All)	*a*	*a*	>360 (All)	*a*	*a*	*a*	115
CL20/HMX/DOS	*a*	*a*	6.419−14.896	*a*	*a*	*a*	*a*	*a*	*a*	44
CL20/HMX/PVAc	*a*	*a*		*a*	*a*		*a*	*a*	*a*	
CL20/HMX/PVB	*a*	*a*		*a*	*a*		*a*	*a*	*a*	
1:1 TT/HNT	*a*	*a*	24	*a*	*a*	80	*a*	*a*	*a*	116
2:1 TT/HDNT	*a*	*a*	>40	*a*	*a*	168	*a*	*a*	*a*	
1:1 TT/TNP	*a*	*a*	32	*a*	*a*	112	*a*	*a*	*a*	
HNTO/AN	*a*	*a*	*a*	*a*	*a*	*a*	*a*	*a*	*a*	117
TNB/1,4-DNI	*a*	14	18	*a*	*a*	*a*	*a*	*a*	*a*	118
TNB/DNMT	*a*	20	22	*a*	*a*	*a*	*a*	*a*	*a*	
CL20/HMX/MF	*a*	*a*	5−15	*a*	*a*	*a*	*a*	*a*	*a*	119
CL20/MTNP	*a*	*a*	4−28	*a*	*a*	60−100	*a*	*a*	*a*	62
HMX/NTO	*a*	*a*	44%	*a*	*a*	40	*a*	*a*	*a*	63
DNP/DAF	*a*	*a*	>40	*a*	*a*	128	*a*	*a*	*a*	32

[a]Not applicable.

the molecular stacking in the crystal (cocrystal).[5] "Turn-on" or "turn off" of the impact sensitivity of EECCs sometimes depends on the stacking, e.g., its impact sensitivity of CL20/TNT[143] decreases by 87%,[133] and in some other cases it increases.[37]

For estimating the extent of the phonon bath (Figure 8) using a physics-based criterion, researchers performed high-quality phonon simulations on 22 molecular crystals. The resulting intrinsic shock sensitivity index (SSI) was then compared to that of the most widely used impact sensitivity marker. Compared to monomolecular crystals, the prediction of sensitivity for cocrystals appears to be more subtle and complicated. Energy transfer rates should most likely be included in up-pumping

https://doi.org/10.1021/acs.cgd.4c00686
Cryst. Growth Des. 2024, 24, 7361−7388

Table 7. Detonation Properties of EECCs of Attractive Nitramines

EECCs (A/B)	D (m/s)			P (GPa)			ref
	A	B	A/B	A	B	A/B	
CL20/BTF	9385	8425	8969	44.9	34.3	39.1	16
CL20/TNT	8770	6712	8426	36.1	19.1	28.7	133
CL20/DNB	9386	5840	8434	45.09	14.18	34.07	18
CL20/TNT	9386	a	8466	45.09	a	33.8	18
CL20/MTNP	9406	8650	9347	44.6	33.7	40.5	19
CL20/AMTN	10117	7108	8863	a	a	a	21
CL20/2,4-MDNI	a	a	8839	a	a	34.82	22
CL20/4,5-MDNI	a	a	8919	a	a	35.69	22
CL20/TNT	8426	6854	8631	a	a	a	54
CL20/DNDAP	9570	7430	8997	44.3	23.4	37.5	42
CL20/TFAZ	9570	8416	9103	44.3	32.9	37.2	29
CL20/2,4-DNI	9687	8136	9324	46	28.1	39.2	34
CL20/1,4-DNI	a	a	9242	a	a	39.01	25
CL20/4,5-MDNI	9386	7455	8604	45.02	23.68	34.45	114
CL20/4,5-MDNI	9386	7455	8972	45.02	23.68	38.59	
HMX/ANPyO	9277	6810	9444	39.87	15.46	41.03	25
HMX/ANPyO	9277	6810	9387	39.87	15.46	40.44	25
HMX/BTNEN	8820	9460	9380	38.54	43.46	42.95	58
CL20/TFAZ	9570	8416	9103	44.3	32.9	37.2	29
CL20/HMX	a	a	a	a	a	a	59
CL20/HMX	a	a	a	a	a	a	60
CL20/MTNI	9767	8360	9093	44.83	30.49	37.46	30
NBA/AmTz, NBA/TATOT, NBA/NPTA, NBA/DAG	a	a	7280; 7521; 6837; 7685	a	a	19.5; 19.7; 17.0; 20.9	115
1:1 TT/HNT	a	a	6091	a	a	a	116
2:1 TT/HDNT	a	a	5884	a	a	a	
1:1 TT/TNP	a	a	6903	a	a	a	
HNTO/AN	a	a	a	a	a	a	117
TNB/1,4-DNI	7277	a	7704	22.4	a	26.08	118
TNB/DNMT	7277	a	7709	22.4	a	22.4	
CL20/HMX/MF	a	a	9200−9250	a	a	a	119
CL20/MTNP	a	a	9347	a	a	40.5	62
HMX/NTO composite	a	a	a	a	a	a	63
DNP/DAF	a	a	a	a	a	a	32

[a]Not applicable.

approaches to cocrystals. Examining the matching lowest frequencies in N−NO_2 stretching modes, they could trigger bond rupture at the corresponding lowest frequencies. After those values are divided by two, the frequencies that remain are those that are associated with N−NO_2 twisting in both CL20 and HMX molecules. Therefore, a vibrational cooling of the N−NO_2 stretching modes by the phonon bath is very likely, depending on the specific mode-to-mode scattering rates, reducing the sensitivity.[146]

The initiation of cocrystals is explained more closely according to Klimenko's and Dremin's "accumulation mechanism"[139] which is also more focused on molecular changes. The kinetic energy of the shock in this compression is accumulated through translational−vibrational relaxation processes by translational and vibrational modes of molecular crystals of the material within 10^{-13} to 10^{-12} s. This change causes considerable quasi-overheating (20000 to 40000 K),[139] particularly in the vibration modes. The energetic substance simultaneously splits into ions and radicals, creating a nonequilibrium state.[139] Through their chemical interactions, these active charged radicals (Figure 8c) cause the shock front to spontaneously spread throughout the initial material, initiating a second equilibrium stage of detonation behind the front. These changes are restricted to the cocrystal active molecular interactions between the coformers. Zeman et al. stated[139] that several authors had used this and related theories of low-frequency crystal lattice vibrations (acoustic phonons) becoming high-frequency vibrations (vibrons), with the subsequent spontaneous localization of vibrational energy in the explosophore groupings,[147,148] in their studies of shock reactivity of energetic materials.

Further, Bernstein correlated experimentally obtained impact sensitivities and FTIR, Raman, and neutron scattering results with vibrational frequencies using plane wave-density functional theory calculations (PW-DFT) and found an excellent correlation between the phonon−vibrational coupling model and experimental impact sensitivities of various secondary explosives. Regardless of the type of secondary explosive, the theoretical approach was proven to be valid for the evaluation of energy transfer rates during the initiation of detonation.[149]

Overall, in the majority of cases, impact sensitivities of EECCs are decreased, and this phenomenal change by cocrystallization grabbed the interest of researchers (Table 6). It is also confirmed that crystal packing−stacking pattern influenced impact; especially, $\pi-\pi$ stacking plays an important role in EECCs achieving low impact sensitivity.[5,150]

5.2. Friction Sensitivity (FS). For FS measurement for EECCs, it is important to note that typical friction generated

https://doi.org/10.1021/acs.cgd.4c00686
Cryst. Growth Des. 2024, 24, 7361−7388

while handling these potentially initiates detonation, and for those EECCs, IS closer to primary explosives must be needed and is highly dependent on the equipment operator. Sometimes, EMs are quite insensitive; however, they are more sensitive to friction, especially energetic salts. FS is also dependent on the morphology and size of CCs, e.g., β-HMX and nano-CCs.[151] HMX/CL20, CL20/RDX showed a significant drop in impact and friction sensitivities.[12,45,53] There is a semilogarithmic relationship between impact and friction sensitivities.[152]

Similarly, in general, EMs with metal oxides like CuO or ZnO with HMX showed reduction in IS but enhancements in FS.[103] Like IS, FS of EECCs, which exhibited rich hydrogen bonds and $\pi-\pi$ stacking, was lower than their pure coformers[5] (Table 6).

5.3. Electrostatic Spark Discharge (ESD). For ESD measurements for EECCs, it is required to note that typical static electricity buildup from everyday activities is in the range of a few millijoules and therefore could potentially initiate detonation and also realize their ESD initiation for technological applications. EECC π-electron excitation effectively causes an ESD response; as for IS and FS, π-stacking plays a significant role in ESD too.[5]

In general, morphologically porous crystals, e.g., porous RDX, with air gaps can exhaust more energy of the ESD spark, and it effectively drops with decreased particle size.[64] In addition, researchers also studied in detail the external electric field influence on EECCs and found that -NO_2 groups trigger bonds on the molecular surface field, i.e., the electric field gradually increases, and the charge of the nitro group gradually increases, indicating that the sensitivity of the EECCs increases.[75,153] An applied electric field triggers the bond in such a way that the direction of the applied positive electric field is defined as N → NO_2, and at the same time, applied negative electric field is defined as NO_2 → N[153] (see Figure 8c). Keeping in mind the technological applications, the sensitivity of EECCs is a significant standard to estimate the safety, and it is mainly defined as the probability for these modified EMs to explode or ignite once subjected to external stimuli, including IS, FS, ESD, shock waves, high temperature, flame combustion etc.[154]

Decreasing the electric spark sensitivity (i.e., increasing the EES values) when the grain size of nitramine crystals increases confirms the idea by Auzanneau et al.[155] about the mechanism of spark energy transfer into the powdered reactive solid, i.e., in this case, decreasing the number of intergrain points in a volume unit. However, there are also dislocations in the crystals that should have some effect on this type of energetic material initiation.[156,157]

6. DETONATION PROPERTIES OF COCRYSTALS

Detonation parameters, detonation velocity (D), detonation pressure (P), and detonation energy (E), are key parameters to evaluate the performance of EECCs (Table 7). Once safety is achieved in sensitive EECCs, their performance needs to be evaluated to comply with technological application suitability.[125] Initial assessment of these parameters includes prediction by software codes like CHEETAH and EXPLO5, Rose Boom etc., using the JCZ3 equation of state[74,112,158,159] and the Kamlet and Jacob equations approach.[160] This key parameter determines the alteration of the detonation power of EECCs and the effectiveness of their initial coformers. D and P will be affected by cocrystallization; the packing density of EECCs is lower; further, it directly influences higher density more promising EMs and also it varies with molar ratios of the coformers chosen for EECC preparations.[71,72]

However, the detonation velocities of a mixture of explosives would be generally higher than what would correspond to the percentage of the components in these mixtures,[161] which is often valid for EECCs also;[127,162,163] in some cases, these properties are increased.[16] Another way it can be described is that it achieves the safety and morphological suitability of EECCs needed to adjust detonation properties slightly; however, it is negligible. It occurs due to the binding energy, trigger bond energy, trigger bond length, and cohesive energy density of EECCs.[164] Earlier reported results showed that between the EECCs and physical mixtures, the crystal structure and resultant coformer bond energy contribute to the observed difference in detonation velocities.[110] Also, researchers studied crystal orientation dependence: (010) crystal orientation is more stable, and the binding energies of the crystal orientations follow the order (010) > (000) > (001) > (100). The detonation performance of PBXs will likely be compromised, given the decrease in density and detonation characteristics.[164]

C−NO_2 linkages need more energy to decompose and detonate than N−NO_2 linkages;[165] when selecting coformers all these facts needs to be considered to obtain better-performing EECCs for military weapons as well as civilian applications. Detonation velocity and detonation pressure are only weakly dependent upon the detonation heat released; it is typically the case for single-component explosives that a high heat of detonation is usually accompanied by a high sensitivity.[77,166] In other words, increasing the fraction of the EM coformer with the highest heat of detonation does not improve the detonation performance (P and D) for some EECCs.[166]

So, overall, it directs research interest in cocrystallization as an attractive strategy to produce decreased sensitivities, which helps to avoid accidental detonation, while maintaining the detonation properties. However, these methodologies still hold some intriguing challenges when it comes to large scale production, which will be discussed in the next section.

7. TECHNOLOGICAL CHALLENGES IN PREPARATION OF COCRYSTALS OF EMS

Despite the widespread use of the cocrystallization approach in the field of EMs, certain investigations are still in the exploratory phase. As a result, some more difficult problems are awaiting solutions.[12,96] As a matter of fact, cocrystallization gives credible productive and cost-effective ways to tune energetic properties of existing EMs instead of undergoing or switching to new molecule synthesis. However, these crystal engineering techniques are fraught with challenges when it comes to large scale preparation to employ defense and civil applications. Although, as discussed in section 2, each preparation method has its pros and cons, researchers are more focused on the scientific part at the laboratory scale due to the availability of EMs and their processing laboratory capacity.

The more important challenge here is scalability; when it comes to large scale production, methods can give good quality of crystals, and at the same time, crystals possibly undergo nucleation and it is difficult maintain required uniform crystalline sizes for their replacement in traditional applications.[52] Obtaining efficient EECCs while maintaining their energy density (bulk energy content), safety, and performance according to the application requirements is also a challenging task.[12,103,167] Especially in terms of their physicochemical and detonation properties, the inherent high sensitivity and high reactivity contributions of EECCs, leading to a discrepancy between the energy content and safety of these EMs, need to be

https://doi.org/10.1021/acs.cgd.4c00686
Cryst. Growth Des. 2024, 24, 7361−7388

achieved while stabilizing them.[50,51,163,168] Sometimes, during cocrystal preparation, the solubility of coformers generally leads to two kinds of crystals with recrystallization without undergoing cocrystallization.[11] Similarly, the morphology of EECCs end up with rod-like or needle-like structures, which makes them unusable in ammunition applications.[169] The field of crystal engineering has so far encountered several obstacles. However, there is no denying that cocrystallization technology will be essential for the creation of the latest forms of EMs, pyrotechnics, and fuel additives.[96] Due to these aspects, the preparation of EECCs according to current application requirements is challenging and tedious; this prompted us to look for an alternative optimized method or modification of an existing method based on earlier groundwork that could be useful for EECC production on large-scale.

At the Institute of Energetic Materials, University of Pardubice, V. B. Patil and S. Zeman tried a shaped and optimized method to modify the EMs and finally developed a universal adaptable strategy with slurry-based coagglomeration in solvent (in which coformers are very little soluble), which is more acceptable safety-wise as well as more effective in tuning energy−safety parameters with controlling their morphology too. Provided structure−property relationships needed to address EECC preparation with respect their coformers, and they will play a very crucial role as backup data and justification to scale up.[175] The VPSZ coagglomeration method (section 7.1) fulfilled all these challenges and successfully developed around 60+ agglomerated crystals (CACs) that form EECCs, and some interesting results have been briefly presented in the upcoming sections.[175]

7.1. Cocrystallization of Nitramines via VPSZ Coagglomeration Method. In this coagglomeration method, coformers DATB, TATB, HNS, HNAB, and BTATz influence the four attractive nitramines RDX, HMX, BCHMX, and CL20. Also, the obtained relationships between impact sensitivity and thermochemical and detonation performance characteristics, on the one hand, and some FTIR and Raman outputs confirm the formation of cocrystals during coagglomeration. All of these mentioned relationships represent new insight into the cocrystal investigation. These instrumental insights are very helpful for analyzing cocrystals that are below 100 μm and not measurable by single crystal X-ray.[108,170−175]

DATB yielded CACs with a density of at most 99% of the theoretical as well as experimental densities of the cocrystals; the TATB CAC densities are higher than those using pure nitramines (including β-CL20). The sensitivity is quite strongly reduced in the TATB CACs (15−50 J) compared with their DATB analogues (4−12 J). Detonation parameters of CACs containing DATB and TATB are logically lower than those of the starting nitramines.[108,171] The CACs with the HNS coformer are finer grained than those with the HNAB one. CACs containing HNAB seem to be more suitable than CACs containing HNS.[172] In the case of BTATz CACs produced parallelly in two batches with a linear stirrer (−B1) and a cross stirrer (+B2), the B2 approach yielded better crystal morphology and quality of surface and higher density,[174] individually discussed in the following sections.

7.1.1. CACs of Attractive Nitramine RDX. RDX showed good compatibility with all coformers, especially with TATB. RDX/TATB showed a high impact resistance of 46.7 J, followed by 10RDX/BTATz B2 (44 J), 17RDX/HNS (20.4 J), and RDX/HNAB (20.5 J) (as shown in Figure 9).[172,174] Also, they had much higher impact resistance than that exhibited by the original pure nitramine. RDX and HMX both showed slightly different intermolecular interactions; $\pi-\pi$ stacking and van der Waals forces dominated, followed by hydrogen bonding, compared to other CACs. It is reversed in other sterically crowded molecules like CL20 and BCHMX.[170] Both thermochemical and detonation properties are preserved as in pure RDX.

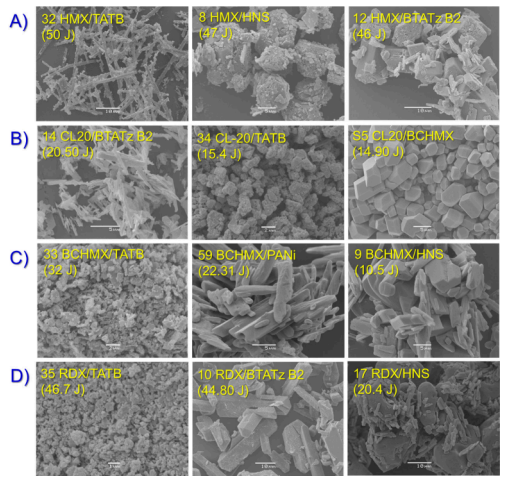

Figure 9. FESEM images with sample IDs of top 3 (left to right) highly impact insensitive CACs. (A) HMX CACs; (B) CL20 CACs; (C) BCHMX CACs; (D) RDX CACs. Images regenerated from earlier publications, refs 106, 108, 170−172, 174). For sample code compositions, see Table 10, and for their impact sensitivities results, see Table 11.

7.1.2. CACs of Attractive Nitramine HMX. HMX showed higher compatibility with all coformers than other nitramines. Especially 32HMX/TATB is highly impact insensitive at 50 J, followed by 8HMX/HNS (47 J) and 12HMX/BTATz (46.01 J) (as shown in Figure 9). Compared to other nitramines, HMX CACs showed very interesting modifications. Both DATB and TATB formed coagglomerates (CACs) with the nitramines, in which HMX is present in its δ-form and CL20 in its β-form;[108,171] the δ-HMX stabilization in these CACs is particularly interesting since the lifetime of the pure isomer is only 12 h.[176] The detonation energies of these mixed crystals are higher than would be expected from the respective percentage of the coformers. The most interesting of the CACs studied appears to be HMX/TATB (D = 9332 m·s^{-1}) which in the formulation used here has a slightly increased density (ρ = 1.909 g·cm^{-3}) with only slightly reduced detonation parameters compared to pure HMX (ρ = 1.902 g·cm^{-3}, D = 9404 m·s^{-1}), while its impact resistance is extremely high (50 J). HMX/HNS at a molar ratio of 1.00/0.11 showed impact sensitivity of 47 J. The study of the surface morphology of these crystals has shown their microporous structure, which is not significantly reflected in their crystal density. These CACs probably contain porous micro/nanocrystalline clusters of HNS (for the pure HNS recently similar structure was described in ref 172).

In these CACs, the HMX is present in its δ-form and CL20 in its β-form, and the trans-HNS molecule changes its conformation to cis-form. On the basis of FTIR and Raman spectral studies, there are more intense intermolecular interactions between HNS and nitramines (especially through the hydrogen bonds formed by the hydrogen atoms of the −CH═CH− bridge), and δ-HMX showed spatial compatibility with cis-HNS molecules. The most interesting CACs from those studied appear to be the already-mentioned HMX/HNS with

https://doi.org/10.1021/acs.cgd.4c00686
Cryst. Growth Des. 2024, 24, 7361−7388

Table 8. Solvent System and Particle Size Measurements

code designation	solvent system of coprecipitation	surface area (m^2/kg)	D_v(50) (μM)	D_v(90) (μM)	ref
32HMX/TATB	DMFA/water	3160	2.45	12.0	171
33BCHMX/TATB	DMFA/water	3765	1.69	12.8	171
34CL20/TATB	DMFA/water	5633	1.77	3.88	171
35RDX/TATB	DMFA/water	4614	12.5	43.1	171
BCHMX/DATB-Cp1	NMP/water	621.1	14.1	33.3	108
BCHMX/DATB-Cp2	NMP/water + surfactant	70.6	127	1809	108
RDX/DATB-Cp3	NMP/water	433.5	23.4	53.3	108
δ-HMX/DATB-Cp4	DMSO/water	665.7	12.1	23.6	108
β-CL20/DATB-Cp5	DMSO/water	1779	22.6	58.1	108
CCs2 CL20/BCHMX	ethyl-formate/hexane	1106	16.9	64.8	170
S4CL20/BCHMX	DMSO/water	1468	15.4	65.2	170
S5CL20/BCHMX	DMSO/water	1007	16.7	50.4	170
S4LV CL20/BCHMX	DMSO/water	861	16.3	58.8	170
S4LZ CL20/BCHMX	DMSO/water	3171	3.22	9.48	170
S5LV CL20/BCHMX	DMSO/water	927	15.6	37.5	170
3HMX/HNS	DMSO/water	1596	5.92	20.1	172
6HMX/HNS	DMSO/water	1973	6.49	26.7	172
8HMX/HNS	DMSO/water	1732	4.52	13.1	172
17RDX/HNS	DMF/water	2089	6.05	23.6	172
18CL20/HNS	DMF/water	1772	8.76	34.2	172
19BCHMX/HNS	DMF/water	1547	6.87	20.2	172
20RDX/HNAB	DMK/hexane	441.3	27.2	54.8	172
21BCHMX/HNAB	DMK/hexane	629.4	19.8	61.8	172
22CL20/HNAB	DMK/hexane	1056	10.8	25.1	172
31HMX/HNAB	DMK/hexane	912.4	15.8	41.9	172
38HMX/HNAB	DMK/hexane	792	15.8	62.9	172
39CL20/HNAB	DMK/hexane	872.9	12.3	33	172
57CL20/PANi	DMSO/water	1764	6.79	40.5	177
58HMX/PANi	DMSO/water	788.6	18.7	80.6	177
59BCHMX/PANi	DMSO/water	1233	8.35	40.1	177
60RDX/PANi	DMSO/water	1126	9.66	40.4	177
9RDX/BTATz B1	dimethyl pyralidone/water	1544	7.79	20.30	174
10RDX/BTATz B2	dimethyl pyralidone/water	2399	3.95	16.80	174
11HMX/BTATz B1	DMSO/water	1034	12.8	29.50	174
12HMX/BTATz B2	DMSO/water	1237	12.2	25.01	174
13CL20/BTATz B1	dimethyl pyralidone/water	1311	16.2	32.10	174
14CL20/BTATz B2	dimethyl pyralidone/water	3154	2.97	6.55	174
15BCHMX/BTATz B1	dimethyl pyralidone/water	1517	7.49	16.90	174
16BCHMX/BTATz B2	dimethyl pyralidone/water	2377	4.52	11.50	174

the molar ratio of 1.00/0.11 and the microporous structure of its crystals, whose calculated detonation velocity is 8.98 km·s^{-1} for ρ = 1.8778 g·cm^{-3} (compare with 9.40 km·s^{-1} for β-HMX). The combination of HMX and HNS molecules thus appears to be advantageous.[172] HMX in the corresponding CACs is present as its α-modification, which is highly sensitive in the pure state (1.9 J). The coagglomerate of α-HMX with BTATz, obtained by coagglomeration under mixing by a cross stirrer, was found to be the least sensitive (46 J) from the studied CACs and should have a detonation energy slightly better than that of β-HMX (6097 vs 5864 J·g^{-1}).[174]

7.1.3. CACs of Attractive Nitramine BCHMX. BCHMX is compatible with these coformers, even though it has a sterically crowded and clipped molecular structure, with particular molar ratios: especially 33BCHMX/TATB showed higher impact insensitivity at 32 J, followed by 16BCHMX/BTATz B2 (11.81 J), and 9BCHMX/HNS (10.5 J) (as shown Figure 9). More interesting is the preparation of the CACs of both sterically crowded coformers CL20/BCHMX with a variation of ratios finally obtaining a stabilized form;[170] in this case, the most important things are the medium used for coagglomeration and the molar ratio of coformers. This modification can yield a cocrystal with clearly lower impact sensitivity (14.9 J for the β-CL20/BCHMX molar ratio = 1.8) than that of pure ε-CL20 (13.2 J) and of pure BCHMX (3 J) (shown in Tables 10 and 11). The density of the studied coagglomerates (CACs) reaches 99.5% of the theoretically calculated ones, and the density of the coformers at the molar ratios used reaches 99.6% of the β-CL20 crystal density. CL20 is present in the CACs as its β-modification; one sample, obtained by classical cocrystallization, has both α- and β-modifications.[170]

The CACs studied have lower detonation energies than would be consistent with the percentage of individual coformers in these crystals; this is a new finding that does not correspond to the general view about the detonation parameters of explosive mixtures. The application of the most sensitive CACs of this type (1.2 J) as a detonator primer did not exhibit the required acceleration capabilities in the given detonator design. However, a comparison with literature data shows that the CACs and CCs of this type could have advantageous applications in propellants because β-CL20 is morphologically stable in these cocrystals.[170]

7.1.4. CACs of Attractive Nitramine CL20. CL20 is the most discussed nitramine molecule in the literature on cocrystallization, with not only energetic materials but also nonenergetic molecules (Tables 6 and 7). Some coagglomerates have shown improved properties, especially 14CL20/BTATz B2 (20.50 J), 34CL20/TATB (15.4 J), and S5 CL20/BCHMX (14.90 J) (as shown in Figure 9). However, for CL20, the entry of HNS or HNAB into its crystal lattice is destabilizing; especially HNAB was not compatible, showing sensitivity like pure CL20.[172] The

https://doi.org/10.1021/acs.cgd.4c00686
Cryst. Growth Des. 2024, 24, 7361−7388

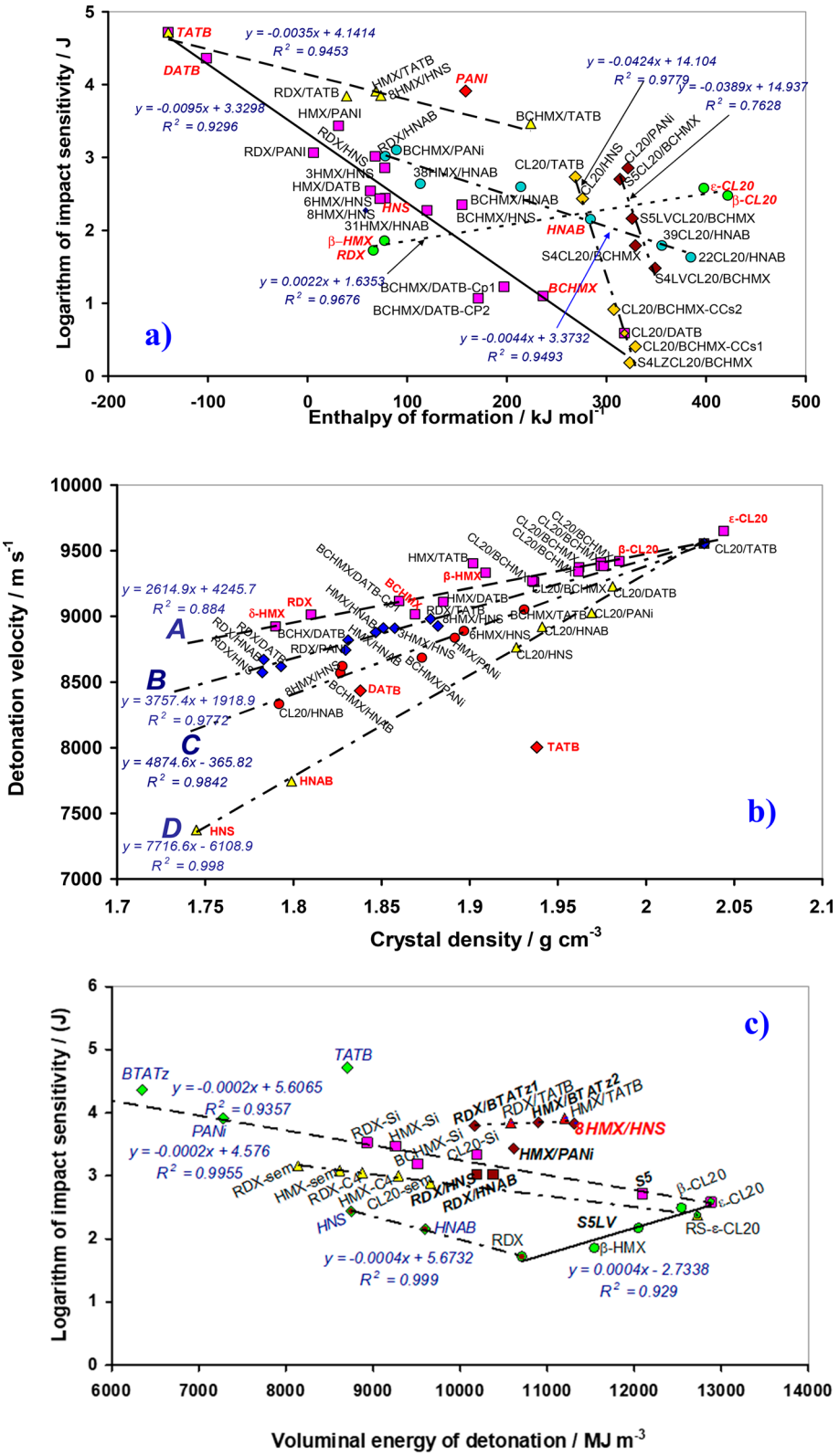

Figure 10. (a) Semilogarithmic relationships between the impact sensitivity and energy content (represented by the enthalpy of formation) of the CACs prepared (data taken from refs 106, 108, 170−172, and 181). (b) Mutual relationships between the calculated detonation velocity for the maximal crystal density and this crystal density (data taken from refs 106, 108, 170−172, 177, and 182). (c) Interesting properties of energetic−energetic cocrystals in comparison with plastic bonded explosives (data taken from refs 106, 108, 170−172, 177, 182, and 183).

most interesting one is with another sterically crowded molecule, CL20, already discussed in BCHMX CACs, section 7.1.3.[170] Most cocrystals in the literature, as well as in the current coagglomeration method when the coformer is a nitro compound, showed phase modification to β-CL20. If the coformer is not a nitro compound, then it switches to γ-CL20.[93]

https://doi.org/10.1021/acs.cgd.4c00686
Cryst. Growth Des. 2024, 24, 7361−7388

Table 9. Summarized Data from DTA Thermograms of Coformers and Cocrystals with Melting Points

samples	melting point (°C)	peaks of changes in DTA record (°C) (with phase modifications) endothermic	exothermic	ref
ε-CL20	240 decompn	170 (ε−γ)	225 (γ−δ)	108
α-CL20	240 decompn	175 (α−γ)	225 (γ−δ)	108
BCHMX	286 decompn		224	108
β-HMX		190 (α−δ)	272	108
α-HMX		189.6 (α−δ)	272	108
RDX	204	209	215	108
DATB	286	230; 290; 295	315; 330	108
TATB		320	357, 365	172
HNS	312−314 decompn	325.41	328.42; 335.25;[a] 340.80[a]	172
HNAB	222−223	134.63; 224.14	335.19; 347.79	177
BTATz		[b]	286.81	184
PANi		[b]	243.25, 246.90, 251.36	171
S32 δ-HMX/TATB		184 (β−δ)	268.85	171
S33 BCHMX/TATB		[b]	225.01	171
S34 β-CL20/TATB		[b]	217.7	171
S35 RDX/TATB		206.18	219.4	108
Cp1 BCHMX/DATB	no melt		227	108
Cp2 BCHMX/DATB	no melt		231	108
Cp3 RDX/DATB	194−195	198	209	108
Cp4 δ-HMX/DATB	242−248	188; 227; 246 (β−δ)	249	108
Cp5 β-CL20/DATB	212−218	176 (β−γ CL20)	216	172
3HMX/HNS		196.54	268; 270.65	172
6HMX/HNS		192.65	267.21	172
8HMX/HNS		192.92	267.21	172
17 RDX/HNS		205.85	221.15	172
18CL20/HNS		[b]	222.45	172
19BCHMX/HNS		[b]	228.5	172
20RDX/HNAB		185.28; 198.23	216.19	172
21BCHMX/HNAB		152.04	215.12	172
22CL20/HNAB		151.32; 223.78	335.36; 350.78[a]	172
31HMX/HNAB		203; 212.36	247.38; 257.66[a]	172
38HMX/HNAB		191.87; 215.10	249.50; 254.02[a]	172
39CL20/HNAB		151.04; 225.28	341.14	170
S4 ($CHCl_3$)		196.01 (β−γ)	214.04 (γ−δ)	170
S5 (BuOH)		200.01 (β−γ)	215.01 (γ−δ)	170
S4LV ($CHCl_3$)		193.75 (β−γ)	218.01 (γ−δ)	170
S4LZ ($CHCl_3$)		200.01 (β−γ)	212.75 (γ−δ)	170
S5LV (BuOH)		198.01 (β−γ)	220.40 (γ−δ)	170
S7CL20/PANi		[b]	218.92	170
S8HMX/PANi		179.4 (β−δ)	265.95	177
S9BCHMX/PANi		[b]	218.53	177
60RDX/PANi		[b]	199.19, 217.56	177
9RDX/BTATz B1		209.25	224.99	177
10RDX/BTATz B2		207.78, 211.90	222.32	184
11HMX/BTATz B1		199.34	251.97	184
12HMX/BTATz B2		193.19	250.81	184
13CL20/BTATz B1		152.74	222.32	184
14CL20/BTATz B2		160.08	217.96	184
15BCHMX/BTATz B1		[b]	226.37	184
16BCHMX/BTATz B2		[b]	213.85	184

[a]Tailing peaks. [b]Not applicable.

Similarly, for example, during the coagglomeration process, ε-CL20 was converted to its β-modification in CL20/BTATz. The cyclic nitramine CACs with nitrogen-rich BTATz as a coformer are exergonic and could provide energy for self-propagating reactions, making them an ideal combination for propulsion applications.[174] Also, both thermochemical and detonation properties are well maintained in CL20 CACs. In addition, the coagglomeration method is compatible with the polymeric moiety polyaniline giving good outputs. All four nitramines showed good interaction with the polymeric chain, giving a unique combination of CACs that are impact insensitive (+5 to 25 J) and electric spark (−100 to 150 mJ) and laser (29 mV with 10×/0.25 grating) sensitive, with relatively better physiochemical properties and detonation properties, especially HMX (to 31 J from original of 6.4 J), which is present in the composite in its α-modification, which in its pure state is extremely sensitive to impact (1.9 J).[175]

7.1.5. Preparation, Morphology, and Particle Size of CACs. As compared to traditional methods of cocrystallization, the coagglomeration method showed improvements in particle sizes of cocrystals, with enhancements in their surface areas (shown in Table 8). The top three highly impact-insensitive cocrystals are shown in Figure 8, which clearly show that at particular molar ratios, the nitramines with energetic coformers have the possibility to achieve the desired impact sensitivity.

General observations found that most CACs showed a decrease in their particle size and increase in their surface area after undergoing coagglomeration (Table 8). Almost all CACs have smooth surfaces with the disappearance of crystal defects, which further influenced improving their impact insensitivity (Figure 9). Also, from the obtained particle size analysis, it was observed that the coagglomeration method yielded fine particles. The trend is uniform in almost all coformers, except in the case of crowded molecules BCHMX and CL20. Angular/clipped structures of BCHMX and globular molecular environments also play a crucial role in crystal growth, which was logically proven.[170]

https://doi.org/10.1021/acs.cgd.4c00686
Cryst. Growth Des. 2024, 24, 7361−7388

Table 10. Molecular Formulas, Thermochemical Properties, and Maximum Crystal Densities of Pure Substances and Their Corresponding CACs

explosive							
code designation	molar ratio NM/CF	formula	mol. weight	Q_c (J·g^{-1})	ΔH_f (kJ·mol^{-1})	ρ (g·cm^{-3})	ref
RDX		$C_3H_6N_6O_6$	222.14	9522	66.2	1.810	108
BCHMX		$C_4H_6N_8O_8$	294.17	9124	236.5	1.860	108
β-HMX		$C_4H_8N_8O_8$	296.18	9485	77.3	1.902	108
β-CL20		$C_6H_6N_{12}O_{12}$	438.23	8327	421.74	1.985	108
ε-CL20		$C_6H_6N_{12}O_{12}$	438,23	8311	397.80	2.044	108
TATB		$C_6H_6N_6O_6$	258.15	11927	−139.74	1.938	108
DATB		$C_6H_5N_5O_6$	243.14	11592	−101.3	1.838	108
HNS		$C_{14}H_6N_6O_{12}$	450.23	11634	78.24	1.745	172
HNAB		$C_{12}H_4N_8O_{12}$	452.21	12384	284.09	1.799	172
PANi		$([C_6H_4NH]_2[C_6H_4N]_2)_n$	95800[185]	24497	158.57	1.5022	177
		$C_{6.00}H_{6.33}N_{0.98}O_{2.00}S_{0.14}$	128.64				
BTATZ		$C_4H_4N_{14}$	248.16	12048	842.10	1.7178	184
32HMX/TATB	1.00:0.12	$C_{4.33}H_{8.00}N_{8.00}O_{8.00}$	300.09	9720	68.80	1.909	171
33BCHMX/TATB	1.00:0.37	$C_{4.86}H_{4.86}N_{8.00}O_{8.00}$	303.33	9335	223.97	1.931	171
34CL20/TATB	1.00:0.17	$C_{7.01}H_{7.01}N_{12.00}O_{12.00}$	451.35	8927	268.76	2.033	171
35RDX/TATB	1.00:0.28	$C_{3.65}H_{5.99}N_{6.00}O_{6.00}$	229.93	9660	39.12	1.869	171
Cp1 BCHMX/DATB	4.20:1.00	$C_{4.72}H_{6.26}N_{8.00}O_{8.19}$	306.44	9627	197.37	1.851	108
Cp2 BCHMX/DATB	3.90:1.00	$C_{4.76}H_{6.27}N_{8.000}O_{8.22}$	307.07	9579	171.46	1.831	108
Cp3 RDX/DATB	3.90:1.00	$C_{3.66}H_{5.76}N_{6.00}O_{6.27}$	234.13	9919	58.33	1.793	108
Cp4 δ-HMX/DATB	3.70:1.00	$C_{4.79}H_{8.00}N_{8.00}O_{8.22}$	309.17	10002	63.10	1.885	108
Cp5 β-CL20/DATB	2.20:1.00	$C_{7.36}H_{7.81}N_{12.00}O_{13.74}$	484.20	9272	318.22	1.981	108
3HMX/HNS	1.00:0.42	$C_{7.54}H_{8.00}N_{8.00}O_{9.93}$	369.56	10880	77.64	1.8730	172
6HMX/HNS	1.00:0.16	$C_{5.57}H_{8.00}N_{8.00}O_{8.85}$	328.60	10386	72.78	1.8820	172
8HMX/HNS	1.00:0.11	$C_{5.09}H_{7.96}N_{8.00}O_{8.57}$	318.32	10055	73.55	1.8778	172
17RDX/HNS	1.00:0.14	$C_{4.35}H_{6.00}N_{6.00}O_{6.73}$	250.02	10040	68.10	1.7824	172
18CL20/HNS	1.00:0.61	$C_{11.14}H_{7.40}N_{12.00}O_{14.80}$	546.15	10444	275.89	1.9265	172
19BCHMX/HNS	1.00:0.25	$C_{5.89}H_{6.31}N_{8.00}O_{9.02}$	333.48	10087	155.11	1.8278	172
20RDX/HNAB	1.00:0.11	$C_{3.90}H_{5.79}N_{6.00}O_{6.00}$	242.32	10033	78.10	1.7831	172
21BCHMX/HNAB	1.00:0.34	$C_{6.44}H_{5.86}N_{8.00}O_{9.62}$	349.23	10138	214.14	1.8267	172
22CL20/HNAB	1.00:0.46	$C_{8.81}H_{6.00}N_{12.00}O_{13.40}$	494.35	9504	384.67	1.7918	172
31HMX/HNAB	1.00:0.185	$C_{5.25}H_{7.37}N_{8.00}O_{8.62}$	320.46	10067	119.90	1.8467	172
38HMX/HNAB	1.00:0.180	$C_{5.22}H_{7.32}N_{8.00}O_{8.53}$	318.61	10046	113.46	1.8575	172
39CL20/HNAB	1.00:0.37	$C_{8.37}H_{6.00}N_{12.00}O_{13.18}$	485.54	9260	355.70	1.9411	172
S4 CL20/BCHMX	1.10:1.00	$C_{6.00}H_{7.23}N_{12.00}O_{12.00}$	439.44	8475	329.00	1.9620	170
S4LV CL20/BCHMX	1.53:1.00	$C_{6.00}H_{6.91}N_{12.00}O_{12.00}$	439.12	8446	348.87	1.9744	170
S4LZ CL20/BCHMX	1.52:1.00	$C_{6.04}H_{6.89}N_{12.00}O_{12.00}$	439.58	8379	323.47	1.9745	170
S5 CL20/BCHMX	1.80:1.00	$C_{6.00}H_{6.78}N_{12.00}O_{12.00}$	438.99	8343	313.62	1.9761	170
S5LV CL20/BCHMX	1.57:1.00	$C_{5.99}H_{6.89}N_{12.00}O_{12.00}$	438.98	8318	325.89	1.9617	170
CCs 1CL20/BCHMX	0.60:1.00	$C_{6.03}H_{7.21}N_{12.00}O_{12.00}$	439.78	8447	329.13	1.9366	170
CCs 2CL20/BCHMX	0.63:1.00	$C_{6.00}H_{7.46}N_{12.00}O_{12.00}$	439.70	8655	307.45	1.9356	170
57CL20/PANi	4.00:1.00	$C_{10.66}H_{11.01}N_{12.00}O_{14.62}S_{0.17}$	546.59	11240	321.47	1.9691	177
58HMX/PANi	4.00:1.00	$C_{6.66}H_{10.16}N_{8.00}O_{9.02}S_{0.13}$	354.58	11979	31.19	1.8967	177
59BCHMX/PANi	4.00:1.00	$C_{6.35}H_{8.00}N_{8.00}O_{8.82}S_{0.05}$	333.40	11245	89.21	1.8916	177
60RDX/PANi	4.00:1.00	$C_{5.09}H_{8.60}N_{6.00}O_{6.71}S_{0.08}$	263.72	12379	6.17	1.8295	177

https://doi.org/10.1021/acs.cgd.4c00686
Cryst. Growth Des. 2024, 24, 7361−7388

Table 10. continued

explosive							
code designation	molar ratio NM/CF	formula	mol. weight	Q_c (J·g^{-1})	ΔH_f (kJ·mol^{-1})	ρ (g·cm^{-3})	ref
9RDX/BTATz B1	1.00:0.20	$C_{2.84}H_{5.16}N_{6.00}O_{4.81}$	200.27	9625	72.37	1.8562	184
10RDX/BTATz B2	1.00:0.21	$C_{2.92}H_{5.38}N_{6.00}O_{5.21}$	207.95	9546	66.50	1.8634	184
11HMX/ BTATz B1	1.00:0.29	$C_{4.36}H_{8.03}N_{8.00}O_{7.80}$	297.28	10229	176.54	1.8835	184
12HMX/ BTATz B2	1.00:0.28	$C_{4.45}H_{7.77}N_{8.00}O_{7.00}$	285.47	10993	276.62	1.8555	184
13CL20/ BTATz B1	1.00:0.45	$C_{6.71}H_{6.92}N_{12.00}O_{10.58}$	424.95	9952	524.14	1.9692	184
14CL20/ BTATz B2	1.00:0.40	$C_{5.66}H_{6.18}N_{12.00}O_{10.13}$	404.40	8787	711.54	2.0041	184
15BCHMX/ BTATz B1	1.00:0.27	$C_{4.35}H_{6.02}N_{8.00}O_{6.64}$	276.59	10177	241.96	1.8341	184
16BCHMX/ BTATz B2	1.00:0.24	$C_{4.87}H_{8.46}N_{8.00}O_{9.13}$	238.64	9975	287.28	1.8697	184

However, coformer TATB has a bigger influence on reducing particle sizes of nitramines due to its strong noncovalent bonds of the N−O−H−N intermolecular interactions. In contrast, DATB does not, and mainly shows $\pi-\pi$ stacking alignments. Also, all coformers showed very good compatibility with HMX and RDX, with both nitramine particle sizes within expectations. In the case of the BTATz CACs, it is interesting to see that the crossed stirrer gives lower particle sizes compared to the linear stirrer, which is used during the coagglomeration process.[106,108,170−172,174]

Further, the coagglomeration method supplies the required force alignment for especially crowded molecules CL20/BCHMX at molar ratio 1.0/1.8 and also surprising impact sensitivity 15 J, which is really good improvement[170] compared to both of its pure coformers' sensitivities. Similarly, in the case of 8δ-HMX/HNS CACs with a molar ratio of 1.00/0.42, in which crystals have a microporous sponge like structure (see SEM images Figure 9) at the same time optimum density is retained. These CACs are highly influenced by coformer HNS, whose final product CAC HMX/HNS also ended with this kind of structure.[172178]

7.1.6. Impact Sensitivity of CACs. The well-known observation of Dr. Licht[140] that high-performance explosives usually have high sensitivity was developed over time into a semilogarithmic relationship[179] between impact sensitivity and the energy content of explosives and the enthalpy of formation, which is presented in Figure 10a.

It is clear that all coformers are stabilized and effectively reduced the impact sensitivity of attractive nitramines, Table 11. Especially, HMX showed more compatibility with all coformers, followed by RDX, BCHMX, and CL20. For both CL20 and BCHMX, as mentioned earlier, due to their crowded molecular environments, it is not easy to interact with selected coformers. However, coagglomeration helped to resolve this problem. In the case of TATB and HNS, SEM images showed that they are imperfect crystals but are highly impact insensitive. It may be due to the flexibility of crystals to withstand impact and form pallets instead of decomposing. To summarize this coagglomeration method effect and output, CAC properties were plotted in dependency graphs using Licht's rule (Figure 10a). The flow of dependencies is consistent, except for pure RDX, HMX, and CL20, for which we needed to find an explanation.[180]

The coformer ratios also play a key role in the variation of impact sensitivity of cocrystals, viz., CL20/BCHMX being both sterically crowded at particular molar ratios (1:1.8) showed higher impact insensitivity.[170] Also, in the case of HNS and HNAB, with slight variation of molar ratios, the impact sensitivity varied.[172] Similarly, the crystallization process during coprecipitation, quick addition of solvent or slow addition of solvent and more importantly, the shape of stirrer factors were well documented.[174]

7.1.7. Thermochemical and Detonation Properties of CACs. The well-known fact that a mixture of two explosives usually produces a higher detonation velocity than would match the amount of components in this mixture is overlooked by researchers studying energetic cocrystals.[158]

It is evident from Table 9 that the onset of the thermal disintegration of CACs is consistently slightly lower than those of pure nitramines. Their exothermic decomposition peak temperatures would also be somewhat lower (Table 9). The mechanism by which the composites interact with the coformer structural components, intermolecular interactions between both coformers as depicted by spectroscopic analysis, may be the cause of the CACs' decreased thermal stability when compared to pure nitramines (also the effect of the mixed melting point has appeared here, which removes the stabilizing effect of the crystalline lattice). This interaction mode is expected to promote the homolysis of the −N−N− in nitramines and −N−O−H− bonds in polynitroarenes with hydrogen atoms in the gamma-position toward the nitro group. Exothermic decomposition occurs in the original thermal range of the CL20 polymorphic transition not only due to the extreme degree of contact in the composite.

Likewise, the decomposition of a composite containing HMX also initiates in the vicinity of its $\alpha-\delta$-transition (in both cases, the movement of molecules in the crystal lattice at the polymorphic transition damages its stabilizing effect). This illustrates how coformers bound to the nitramines started to break down in this CACs solid form, which is significantly different from how CACs are thermolyzed with polynitro compounds.

The data in Figure 10b shows that group A's brisant explosives (primarily CL20 and partially BCHMX) have the least impact on the increase in E_{deton} values for the CACs, and group B's CACs of RDX and HMX with coformers have higher increases

https://doi.org/10.1021/acs.cgd.4c00686
Cryst. Growth Des. 2024, 24, 7361−7388

Table 11. Impact Sensitivity and Explosive Properties of Pure Substances and Corresponding CACs

code designation	impact sensitivity E_{dr}(50%) (J)	impact sensitivity E_{dr}(95%) (J)	D (m·s^{-1})	P (Gpa)	E_{deton} (J·g^{-1})	additive value[a] of E_{deton} (J·g^{-1})	ref
RDX	5.6		9014	33.91	5915		108
BCHMX	3.0		9116	36.19	6223		108
β-HMX	6.4		9404	38.00	5964		108
β-CL20	11.9[b]		9421	40.77	6320		108
ε-CL20	13.2;[b] 4.0[c]		9650	43.41	6303		108
DATB	78.5		8004	27.13	4086		108
TATB	112.0		8434	31.01	4492		108
HNS (form I)	11.5		7373	22.81	5015		172
HNAB	8.6		7744	26.12	5335		172
PANi	50.0	108.0	6813	16.61	6813	4845	177
BTATZ	78.50	93.62	7291	20.41	3695	7291	184
32HMX/TATB	50.0	98.3	9332	37.73	5867	5817	171
33BCHMX/TATB	32.0	76.0	9051	36.75	5931	5798	171
34CL20/TATB	15.4	41.1	9556	42.60	6265	5788	171
35RDX/TATB	46.7	71.5	9016	34.86	5662	5569	171
Cp1 BCHMX/DATB	3.4	8.8	8913	34.45	5952	5872	108
Cp2 BCHMX/DATB	2.9	6.0	8819	33.50	5915	5849	108
Cp3 RDX/DATB	9.7	20.0	8619	31.61	5621	5589	108
Cp4 δ-HMX/DATB	12.7	97.2	9111	35.78	5730	5630	108
Cp5 β-CL20/DATB	1.8	2.1	9229	38.88	5978	5869	108
3HMX/HNS	17.4	35.0	8685	33.03	5637	5592	172
6HMX/HNS	11.4	17.6	8927	34.45	5778	5773	172
8HMX/HNS	47.0	105.1	8982	34.73	5804	5819	172
17RDX/HNS	20.4	47.0	8572	30.95	5720	5717	172
18CL20/HNS	11.4	18.6	8764	35.01	5961	5815	172
19BCHMX/HNS	10.5	24.4	8622	32.13	5780	5891	172
20RDX/HNAB	20.5	46.4	8671	31.66	5822	5807	172
21BCHMX/HNAB	13.4	39.2	8568	32.01	5894	5918	172
22CL20/HNAB	5.1	11.4	8333	30.11	5791	6000	172
31HMX/HNAB	9.7	34.8	8879	33.96	5842	5824	172
38HMX/HNAB	14.0	37.5	8911	34.30	5817	5828	172
39CL20/HNAB	6.0	28.5	8921	36.17	5924	5786	172
S4 CL20/BCHMX	6.0	8.4	9373	39.65	6163	6273	170
S4LV CL20/BCHMX	4.4	8.6	9410	40.20	6198	6279	170
S4LZ CL20/BCHMX	1.2	4.9	9385	39.94	6136	6278	170
S5 CL20/BCHMX	14.9	38.5	9383	39.93	6123	6281	170
S5LV CL20/BCHMX	8.7	20.8	9341	39.41	6143	6279	170
CCs1 CL20/BCHMX	1.5		9262	38.43	6139	6261	170
CCs2 CL20/BCHMX	2.5		9268	38.39	6113	6262	170
57CL20/PANi	17.4	33.4	9025	38,05	5971	5971	177
58HMX/PANi	31.0	87.2	8890	35.3	5597	5597	177
59BCHMX/PANi	22.3	55.9	8836	34.58	5638	5638	177
60RDX/PANi	21.4	31.1	8744	33.26	5544	5544	177
9RDX/BTATz B1	44.50	71.41	8974	34.08	5478	71.41	184
10RDX/BTATz B2	44.80	69.10	9063	34.93	5627	69.10	184
11HMX/BTATz B1	44.16	64.60	9305	37.45	6098	64.60	184
12HMX/BTATz B2	46.01	51.95	9167	36.17	6097	51.95	184
13CL20/BTATz B1	18.31	46.72	9290	39.40	61.51	46.72	184
14CL20/BTATz B2	20.50	25.06	9643	43.30	6633	25.06	184
15BCHMX/BTATz B1	10.41	20.01	8810	33.25	5755	20.01	184
16BCHMX/BTATz B2	11.81	18.06	8857	33.78	5497	18.06	184

[a]Value calculated on the basis of the additive principle, i.e., percentage of components in the coagglomerate. [b]Values for pure β-CL20 and ε-CL20, respectively, taken from ref 186. [c]Value for "common" (technical) quality ε-CL20.

in these values. Group C, PANi coformer, has the largest effect ever observed.

The data from Table 11 show that CACs 39CL-20/HNAB, S4 CL20/BCHMX, S4LV CL20/BCHMX, S4LZ CL20/BCHMX, S5 CL20/BCHMX, S5LV CL20/BCHMX, and CCs1 CL20/BCHMX appear to form a single intersection where all dependencies seem to meet. The combination has the opposite effect on these nitraminic CACs alone. According to Prof. Urbanski, increases in these detonation values are caused by the coformers entering the combination having more entropy.[161]

https://doi.org/10.1021/acs.cgd.4c00686
Cryst. Growth Des. 2024, 24, 7361−7388

Concerning the nitramine CACs, it is determined that the decrease in the E_{deton} values was caused by the entropy in the mixing of chemically identical but admittedly structurally different coformers.[170] Figure 10b shows the well-known correlation between the explosive charge densities and detonation velocities. Group A, which consists primarily of pure nitramines (extremely brisant explosives), is followed by groups B and C, which contain RDX, BCHMX, and HMX coagglomerates. Group C, which includes both pure HNAB and HNS as well as CACs with CL20 content, is characterized by a significantly reduced detonation velocity due to the coformers HNS, HNAB, PANi, and DTAB. It can be observed that HMX/TATB, as shown in Table 11, which exhibits strong resistance to impact, ought to possess a detonation velocity that is comparable to that of pure β-HMX. δ-HMX/cis-HNS, another CAC more resistant to impact (Table 11), is similar to pure RDX.

7.1.8. Feasibility of Coagglomeration Method. The initiation reactivity of attractive nitramines is typically decreased upon adding polynitro compound molecules to their crystal lattice, particularly for molecules that are densely packed. However, this effect can be mitigated by carefully choosing the molar ratio of the resulting CACs, as demonstrated by previous findings.[106,108,170−172,177,182] So far, TATB has proven to be the most effective "stabilizer" among these nitramines. Interestingly, the coformer cis-HNS has a comparable impact on δ-HMX stabilization (even if the molar ratio of the coformers is crucial in this case). In addition, the microporosity of cis-HNS in the final CACs can prove to be a noteworthy beneficial component. The δ-HMX/TATB coagglomerate is the most beneficial from the perspective of explosive properties, with performance that is comparable to pure β-HMX. Likewise, pure RDX and the optimal coagglomerate δ-HMX/cis-HNS are logically close in terms of performance.

Coagglomeration is generally categorized theoretically as the "slurry method" of cocrystallization, which involves preparing cocrystals and yields highly intriguing energetic materials with a relatively high crystal density. One can use components straight from production after isolating them from reaction mixes and stabilizing them. Thus, there is no need for initial coformers with a defined granulometry. Coformers can be co-precipitated to purify themselves in solution.

The initial findings imply that,[182] similar to traditional crystallization, chemical engineering considerations play a role in the CAC preparation process. This technology can be used for industrial scale cocrystal manufacturing with the help of technical and technological optimization.

8. CONCLUDING REMARKS

In essence, every practical technological procedure for cocrystallization of energetic materials relies on a bottom-up approach; energy−safety balanced energetic materials (with desirable thermochemical and stability characteristics) can be achieved. In cocrystallization, both energetic conformers undergo noncovalent self-assembly with supramolecular interactions, like hydrogen bonding, $\pi-\pi$ stacking, van der Waals forces, etc. These interactions play a key role in influencing the energetic properties of cocrystals. In this way, cocrystallization can increase their applicability in various types of military and civilian technical applications. Key highlights of this review are summarized in the following sections.

8.1. Key Factors Influence in Cocrystallization of Energetic Materials.

- Generally, strong hydrogen bonds are shorter, which strongly influences the formation of stable cocrystals (two types - strong and weak).
- Normally, the distances of intermolecular forces (van der Waals interactions and HBs) are in the range of 3.10−5.03 Å and 1.10−3.10 Å.
- The interaction of a lone pair of one coformer with the π-structure of another is referred to as n$-\pi$ stacking, and similarly, if both interacting conformers have π structure, it denoted as $\pi-\pi$ stacking. These π-stacking interactions between -NO_2 groups and aromatic rings form herringbone-like structures via stacking groups.
- Crystal packing changes actively influence intermolecular arrangement and respond to stimuli via converting mechanical to intermolecular interaction energy, which disperses throughout stacked layers of the EECCs in the following ascending order: wavelike (layer-by-layer), crossed (caged), face-to-face (sandwich), and mixed stackings.
- Cocrystallization alters physicochemical behavior, including melting and decomposition temperatures (±5−20 °C) based on intermolecular interactions and crystal packing. The stacking conditions in the crystal lattice of EECCs significantly contribute to this effect, and the density gained by these intermolecular interactions is defined as cohesive energy density (CED).
- In most of the cases (99%), impact sensitivities of EECCs are decreased, and this phenomenal change made cocrystallization interesting for researchers.
- The detonation velocity (D) and detonation pressure (P) will be affected by cocrystallization through the packing density of EECCs, i.e., by more promising values of D due to higher crystal density, depending on the molar ratios of the coformers chosen for the preparation of EECCs.
- However, the detonation velocities of explosive mixtures would generally be higher than that of coformers in these cocrystals, which is often the case for EECCs. In some cases, the effect could be more pronounced for cocrystals, but the opposite effect has been observed for nitramine EECCs.
- Another way of describing the achievement of safety and morphological suitability of EECCs is the slight variation in their detonation properties, but this is negligible. It occurs due to the binding energy, trigger energy, trigger bond length, and cohesive energy density of EECCs.

8.2. Cocrystallization with Traditional Cocrystallization Methods.

- Traditional cocrystallization gives good scientific context and background exposition to continue trials with new method developments.
- The evaporation method is mainly good for determining the compatibility of the molar ratio of both coformers by growing a single crystal and further thoroughly analyzing it.
- Spray drying is also good for laboratory as well as large-scale preparations; however, maintaining higher pressure and hot walls is challenging for energetic materials and not cost-effective for continuous production.
- Slurry techniques are better for the cocrystallization of energetic materials; crystallization in a solution medium can be controlled by varying the solution addition, mixing,

https://doi.org/10.1021/acs.cgd.4c00686
Cryst. Growth Des. 2024, 24, 7361−7388

and stirring. It provides more possibilities more safety; it seems most effective for energetic materials.

- Vacuum freeze-drying is also, like the evaporation method, more effective for laboratory scale cocrystallization of energetic materials that do not easily undergo cocrystallization. It also needs higher-scale maintenance and is not cost-effective for larger-scale preparation.
- So, traditional methods lack affordable scalability when it comes to energetic materials, so researchers are still looking for new or modified methods of preparation.

8.3. Cocrystallization via Coagglomeration.

- This method is practically an innovated cocrystallization in suspension, generally classified in the literature as the "slurry method", which considerably reduces the processing time and decreases the quantity of solvents compared to a solvent cocrystallization. It provides fine cocrystals of very good quality.
- The newly applied proven spectroscopic methods correlate their outputs with the molecular and utility characteristics of the cocrystals. These coagglomerated crystals have been characterized by instrumental analysis techniques such as PXRD, FTIR, and Raman spectroscopy; the results obtained in all cases are fully consistent, showing very interesting correlations, with the current knowledge of the types of intermolecular interactions in the crystals and the relative property changes that occur in these types of cocrystals.
- The coagglomeration method also showed the higher importance of coformer molecular ratio, preparation, selections, etc., and also their influence on the thermochemical and detonation properties of obtained cocrystals.
- Cocrystals showed tremendously improved properties as compared to earlier traditional cocrystallization methods with uniform-size crystallization and proved that the coagglomeration method is suitable for larger scale preparations

8.4. Future Applications of Cocrystals.

- For the individual coformers chosen for the preparation of cocrystals of attractive nitramines, the future applications are addressed on the basis of their interesting characteristic thermochemical and energetic properties.
- These are suitable fillers in insensitive ammunition and secondary fillers of detonators for deep holes.
- Cocrystals provide energy for self-propagating reactions for spacecraft, making them an ideal combination for propulsion applications and also ammunition and special charges.
- Also, they are suitable for catapulting charges with a combination of other CACs as main charges, i.e., application of electromagnetic launch technology in the field of missiles.

This review showed the impacts of various traditional preparation methods of cocrystallization and characteristics compared with the VPSZ coagglomeration method. The VPSZ coagglomeration process is more promising, is expected to continue advancing, and will keep advancing at the technology level in upcoming years.

AUTHOR INFORMATION

Corresponding Author

Veerabhadragouda B. Patil − *Institute of Energetic Materials, Faculty of Chemical Technology, University of Pardubice, CZ532 10 Pardubice, Czech Republic;* orcid.org/0000-0001-9410-6524; Email: iamveerabhadraa@gmail.com

Author

Svatopluk Zeman − *Institute of Energetic Materials, Faculty of Chemical Technology, University of Pardubice, CZ532 10 Pardubice, Czech Republic;* orcid.org/0000-0001-8003-9690

Complete contact information is available at: https://pubs.acs.org/10.1021/acs.cgd.4c00686

Notes

The authors declare no competing financial interest.

Biographies

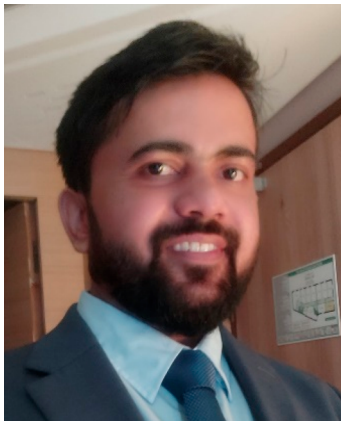

Veerabhadragouda B. Patil completed his Ph.D., under the supervision of Prof. Svatopluk Zeman at the Institute of Energetic Materials, Faculty of Chemical Technology, University of Pardubice, Czech Republic (2020−2024). His research work focuses on achieving Energy−Safety balanced energetic materials. During his Ph.D. studies, he completed two Erasmus+ internships, one at Łukasiewicz Research Network − Institute of Industrial Organic Chemistry, Warszawa (2022), Poland, and another at Department of Chemistry and Biochemistry, Ludwig-Maximilian University of Munich, Munich, Germany (2023). He has two years of GUG-PEL Project (funded by Premier Explosives Ltd. Hyderabad, India) experience (2018−2019). Furthermore, he has two years of working experience as a Quality Assurance officer at Cipla Ltd, India (Pharmaceutical company-API unit) (2015−2017). He completed his M.Sc. from the Karnataka University, Dharwad, India (2013−2015), in Chemistry with an academic project and also, a summer research project at CSIR-National Chemical Laboratory, Pune, India (2014). He has published 50+ journal and conference research articles, with more than 650+ Google Scholar citations with an h-index of 15. He also has prestigious memberships in the scientific societies: Indian Chromatographic Society (2018−), American Chemical Society (2020−), Royal Society of Chemistry (MRSC) (2022−), and German Chemical Society (GDCh) (2023−).

https://doi.org/10.1021/acs.cgd.4c00686
Cryst. Growth Des. 2024, 24, 7361−7388

Svatopluk Zeman (b 1942), received his M.Sc. in Technology of explosives from the University of Pardubice in 1966. He completed his Ph.D. in 1972; due to political reasons, it was defended in 1989. In the 1969−1993 period, he was a researcher in the Slovak enterprise Chemko Strážske. In November 1992, he was appointed Associate Professor and in February 1993, he returned to this University. In 1998 he defended his D.Sc. Thesis at the University of Chemistry and Chemical Technology in Prague, and in 2000, he was appointed full Professor of Organic Technology − Technology of Explosives. In the 1994−2015 period, he was a head of the Institute of Energetic Materials at the University of Pardubice. He has coauthored about 175+ papers in impacted journals, around 80+ contributions at conferences and more than 175 patents (his Scopus's h-index is 31 with 3350+ citations, self-citations excluded), from June 2016 appearing in the "World's Top 2% most cited scientists" (Stanford Univ. & Elsevier). His research focuses on the initiation reactivity of energetic materials and technological aspects of new explosives. He was cofounder and, from 1999 until 2022, chairman of the International Seminars called "New Trends in Research of Energetic Materials" which are organized at University of Pardubice (www.ntrem.com).

■ ABBREVIATIONS

α-, β-, γ-, ε- and δ-HMX	polymorphic modifications of 1,3,5,7-tetranitro-1,3,5,7-tetrazocane
α-, β-, γ-, ε- and δ-CL20	polymorphic modifications of 2,4,8,10,12-hexanitro-2,4,8,10,12-hexazaisowurtzitane
ΔH_f	enthalpy of formation
Q_c	heat of combustion
P	detonation pressure
D	detonation velocity
E_{deton}	energy of detonation,
$D_v(50)$	50% of the cumulative volume distribution of particles
$D_v(90)$	90% of the cumulative volume distribution of particles
$E_{dr}(50\%)$	impact sensitivity expressed as drop energy for 50% probability of initiation
$E_{dr}(95\%)$	impact sensitivity expressed as drop energy for 95% probability of initiation
L	large-scale
P	co-precipitate
CC	cocrystal
CAC	coagglomerated crystal
CF	coformer
EECC	energetic−energetic cocrystal
LOVA	low vulnerability ammunition
PM	physical mixture
PXRD	powder X-ray diffraction
FESEM	field emission scanning electron microscopy
FTIR	Fourier transform infrared spectroscopy
DTA	differential thermal analysis
DSC	differential scanning colorimetry
TGA	thermogravimetric analysis
DMA	dynamic mechanical analysis
1,4-DNI	1,4-dinitroimidazole
2,4-DNI	2,4-dinitroimidazole
4,5-MDNI	4,5-dinitro-1-methylimidazole
ADNP	4-amino-3,5-dinitropyrazole
AMTN	1-amino-3-methyl-1,2,3-triazolium-nitrate
ANPyO	2,6-diamino-3,5-dinitropyridine-1-oxide
AN	ammonium nitrate
AP	ammonium perchlorate
aTRz	Azo-bis-1,2,4-triazole
BCHMX	1,3,4,6-tetranitrooctahydroimidazo-[4,5-*d*]imidazole
BTF	benzotrifuroxane
BTNEN	1,2,4-butanetriol trinitrate
CAM	ε-caprolactone monomer
CL20	2,4,6,8,10,12-hexanitro-2,4,6,8,10,12-hexaazaisowurtzitane (also referred to as HNIW)
DADP	diacetone diperoxide
DAF	3,4-diaminofurazan
DATB	1,3-diamino-2,4,6-trinitrobenzene
DMF	dimethyl formaldehyde
DMSO	dimethyl sulfoxide
DNB	dinitrobenzene
DNBT	5,5′-dinitro-2*H*,2*H*′-3,3′-bi-1,2,4-triazole
DNDAP	2,4-dinitro-2,4-diazapentane
DNI	dinitroimidazole
DNMT	1-methyl-3,5-dinitro-1,2,4-triazole
DNP	2,4-dinitrophenol
DNT	1-methyl-2,4-dinitrobenzene
FOX-7	1,1-diamino-2,2-dinitroethene
H_2O_2	hydrogen peroxide
HB	hydrogen bond
HEDM	high energy density material
HMPT	hexamethylphosphoramide
HMX	1,3,5,7-tetranitro-1,3,5,7-tetraazacyclooctane
HNAB	2,2′,4,4′,6,6′-hexanitroazobenzene
HNTO	hydrazine 3-nitro-1,2,4-triazol-5-one
HNS	2,2′,4,4′,6,6′-hexanitrostilbene
HTPB	hydroxyl-terminated polybutadiene
MDNT	1-methyl-3,5-dinitro-1,2,4-triazole
MTNI	1-methyl-3,5-dinitro-1,2,4-imidazole
MTNP	1-methyl-3,4,5-trinitropyrazole
n-K6	2-oxo-1,3,5-trinitro-1,3,5-triazacyclohexane, also known as K6 or Keto-RDX
NC	nitrocellulose
NM	nitromethane
NMP	*N*-methyl-2-pyrrolidone

https://doi.org/10.1021/acs.cgd.4c00686
Cryst. Growth Des. 2024, 24, 7361−7388

N−O···H	hydrogen bonding
NT	nitrotoluene
NTO	3-nitro-1,2,4-triazol-5-one
PANi	polyaniline
PETN	pentaerythritol tetranitrate
PVAc	poly(vinyl acetate)
RDX	1,3,5-trinitro-1,3,5-triazacyclohexane
TATB	1,3,5-triamino-2,4,6-trinitrobenzene
TATP	triacetone triperoxide
TCTNB	1,3,5-trichloro-2,4,6-trinitrobenzene
TEX	4,10-dinitro-2,6,8,12,-tetraoxa-4,10-diazasowurtzitane
TFAZ	7*H*-trifurazano[3,4-*b*:3′,4′-*f*:3″,4″-*d*]azepine
TMS	tetramethylene sulfone
TNAZ	1,3,3-trinitroazetidine
TNP	1,3,5-trinitro-1,3-diazacyclohexane
TNT	2,4,6-trinitrotoluene

REFERENCES

(1) Agrawal, J. P. *High Energy Materials: Propellants, Explosives and Pyrotechnics*, 1st ed.; Wiley, 2010; DOI: 10.1002/9783527628803.

(2) Elbeih, A. I. M.; Husarova, A.; Zeman, S. Method of Preparation of ε-2,4,6,8,10,12-Hexanitro-2,4,6,8,10,12-Hexaazaisowurtzitane with Reduced Impact Sensitivity. International Patent WO2013044891A1, April 4, 2013.

(3) Deplancke, T.; Lame, O.; Rousset, F.; Aguili, I.; Seguela, R.; Vigier, G. Diffusion versus Cocrystallization of Very Long Polymer Chains at Interfaces: Experimental Study of Sintering of UHMWPE Nascent Powder. *Macromolecules* **2014**, *47* (1), 197−207.

(4) Bennion, J.; McBain, A.; Son, S.; Matzger, A. Design and Synthesis of a Series of Nitrogen-Rich Energetic Cocrystals of 5,5′-Dinitro-2H,2H′-3,3′-Bi-1,2,4-Triazole (DNBT). *Cryst. Growth Des.* **2015**, *15* (5), 2545−2549.

(5) Bu, R.; Xiong, Y.; Zhang, C. Pi-Pi Stacking Contributing to the Low or Reduced Impact Sensitivity of Energetic Materials. *Cryst. Growth Des.* **2020**, *20* (5), 2824−2841.

(6) Aitipamula, S.; Banerjee, R.; Bansal, A. K.; Biradha, K.; Cheney, M. L.; Choudhury, A. R.; Desiraju, G. R.; Dikundwar, A. G.; Dubey, R.; Duggirala, N.; Ghogale, P. P.; Ghosh, S.; Goswami, P. K.; Goud, N. R.; Jetti, R. R. K. R.; Karpinski, P.; Kaushik, P.; Kumar, D.; Kumar, V.; Moulton, B.; Mukherjee, A.; Mukherjee, G.; Myerson, A. S.; Puri, V.; Ramanan, A.; Rajamannar, T.; Reddy, C. M.; Rodriguez-Hornedo, N.; Rogers, R. D.; Row, T. N. G.; Sanphui, P.; Shan, N.; Shete, G.; Singh, A.; Sun, C. C.; Swift, J. A.; Thaimattam, R.; Thakur, T. S.; Kumar Thaper, R.; Thomas, S. P.; Tothadi, S.; Vangala, V. R.; Variankaval, N.; Vishweshwar, P.; Weyna, D. R.; Zaworotko, M. J. Polymorphs, Salts, and Cocrystals: What's in a Name? *Cryst. Growth Des.* **2012**, *12* (5), 2147−2152.

(7) Bennion, J.; Matzger, A. Development and Evolution of Energetic Cocrystals. *Acc. Chem. Res.* **2021**, *54* (7), 1699−1710.

(8) Liu, G.; Wei, S.; Zhang, C. Review of the Intermolecular Interactions in Energetic Molecular Cocrystals. *Cryst. Growth Des.* **2020**, *20* (10), 7065−7079.

(9) Ren, C.; Liu, H.; Li, X.; Guo, L. Decomposition Mechanism Scenarios of CL-20 Co-Crystals Revealed by ReaxFF Molecular Dynamics: Similarities and Differences. *Phys. Chem. Chem. Phys.* **2020**, *22* (5), 2827−2840.

(10) Feng, R.; Zhang, S.; Ren, F.; Gou, R.; Gao, L. Theoretical Insight into the Binding Energy and Detonation Performance of Epsilon-, Gamma-, Beta-CL-20 Cocrystals with Beta-HMX, FOX-7, and DMF in Different Molar Ratios, as Well as Electrostatic Potential. *J. Mol. Model.* **2016**, *22* (6), 123.

(11) Wiscons, R.; Matzger, A. Evaluation of the Appropriate Use of Characterization Methods for Differentiation between Cocrystals and Physical Mixtures in the Context of Energetic Materials. *Cryst. Growth Des.* **2017**, *17* (2), 901−906.

(12) Xue, Z.; Huang, B.; Li, H.; Yan, Q. Nitramine-Based Energetic Cocrystals with Improved Stability and Controlled Reactivity. *Cryst. Growth Des.* **2020**, *20* (12), 8124−8147.

(13) Liu, N.; Duan, B.; Lu, X.; Mo, H.; Bi, F.; Wang, B.; Zhang, J.; Yan, Q. Rapid and High-Yielding Formation of CL-20/DNDAP Cocrystals via Self-Assembly in Slightly Soluble-Medium with Improved Sensitivity and Thermal Stability. *Propellants Explosives Pyrotechnics* **2019**, *44* (10), 1242−1253.

(14) Zhang, J.; Hooper, J.; Zhang, J.; Shreeve, J. Well-Balanced Energetic Cocrystals of H5IO6/HIO3 Achieved by a Small Acid-Base Gap. *Chemical Engineering Journal* **2021**, *405*, 126623.

(15) Bolton, O.; Matzger, A. J. Improved Stability and Smart-Material Functionality Realized in an Energetic Cocrystal. *Angew. Chem., Int. Ed.* **2011**, *50* (38), 8960−8963.

(16) Yang, Z.; Li, H.; Zhou, X.; Zhang, C.; Huang, H.; Li, J.; Nie, F. Characterization and Properties of a Novel Energetic-Energetic Cocrystal Explosive Composed of HNIW and BTF. *Cryst. Growth Des.* **2012**, *12* (11), 5155−5158.

(17) Aldoshin, S. M.; Aliev, Z. G.; Goncharov, T. K.; Kazakov, A. I.; Milekhin, Yu. M.; Plishkin, N. A.; Shishov, N. I. Structure and Properties of Cocrystals of Trinitrotoluene and 2,4,6,8,10,12-Hexanitro-2,4,6,8,10,12-Hexaazaisowurtzitane. *Russ Chem. Bull.* **2013**, *62* (6), 1354−1360.

(18) Wang, Y.; Yang, Z.; Li, H.; Zhou, X.; Zhang, Q.; Wang, J.; Liu, Y. A Novel Cocrystal Explosive of HNIW with Good Comprehensive Properties. *Propellants, Explosives, Pyrotechnics* **2014**, *39* (4), 590−596.

(19) Ma, Q.; Jiang, T.; Chi, Y.; Chen, Y.; Wang, J.; Huang, J.; Nie, F. A Novel Multi-Nitrogen 2,4,6,8,10,12-Hexanitrohexaazaisowurtzitane-Based Energetic Co-Crystal with 1-Methyl-3,4,5-Trinitropyrazole as a Donor: Experimental and Theoretical Investigations of Intermolecular Interactions. *New J. Chem.* **2017**, *41* (10), 4165−4172.

(20) Gao, H.; Jiang, W.; Liu, J.; Hao, G.; Xiao, L.; Ke, X.; Chen, T. Synthesis and Characterization of a New Co-Crystal Explosive with High Energy and Good Sensitivity. *Journal of Energetic Materials* **2017**, 1−9.

(21) Zhang, X.; Chen, S.; Wu, Y.; Jin, S.; Wang, X.; Wang, Y.; Shang, F.; Chen, K.; Du, J.; Shu, Q. A Novel Cocrystal Composed of CL-20 and Energetic Ionic Salt. *Chem. Commun.* **2018**, *54*, 13268−13270.

(22) Yang, Z.; Wang, H.; Ma, Y.; Huang, Q.; Zhang, J.; Nie, F.; Zhang, J.; Li, H. Isomeric Cocrystals of CL-20: A Promising Strategy for Development of High-Performance Explosives. *Cryst. Growth Des.* **2018**, *18* (11), 6399−6403.

(23) Zhu, S.; Zhang, S.; Gou, R.; Wu, C.; Han, G.; Jia, H. Understanding the Effect of Solvent on the Growth and Crystal Morphology of MTNP/CL-20 Cocrystal Explosive: Experimental and Theoretical Studies. *Crystal Research and Technology* **2018**, *53* (4), 1700299.

(24) Sun, S.; Zhang, H.; Liu, Y.; Xu, J.; Huang, S.; Wang, S.; Sun, J. Transitions from Separately Crystallized CL-20 and HMX to CL-20/HMX Cocrystal Based on Solvent Media. *Cryst. Growth Des.* **2018**, *18* (1), 77−84.

(25) Tan, Y.; Yang, Z.; Wang, H.; Li, H.; Nie, F.; Liu, Y.; Yu, Y. High Energy Explosive with Low Sensitivity: A New Energetic Cocrystal Based on CL-20 and 1,4-DNI. *Cryst. Growth Des.* **2019**, *19* (8), 4476−4482.

(26) Sun, S.; Zhang, H.; Xu, J.; Wang, H.; Wang, S.; Yu, Z.; Zhu, C.; Sun, J. Design, Preparation, Characterization and Formation Mechanism of a Novel Kinetic CL-20-Based Cocrystal. *Acta Crystallogr. B Struct Sci. Cryst. Eng. Mater.* **2019**, *75* (3), 310−317.

(27) Fei, T.; Lv, P.; Liu, Y.; He, C.; Sun, C.; Pang, S. Design and Synthesis of a Series of CL-20 Cocrystals: Six-Membered Symmetrical N-Heterocyclic Compounds as Effective Coformers. *Cryst. Growth Des.* **2019**, *19* (5), 2779−2784.

(28) Liu, Y.; Lv, P.; Sun, C.; Pang, S. Syntheses, Crystal Structures, and Properties of Two Novel CL-20-Based Cocrystals. *Zeitschrift fur Anorganische und Allgemeine Chemie* **2019**, *645* (8), 656−662.

(29) Liu, N.; Duan, B. H.; Lu, X. M.; Wang, B. Z. Investigation of CL-20/TFAZ Cocrystal: Preparation, Structure and Performance. *J. Phys.: Conf. Ser.* **2021**, *1721* (1), 012005.

https://doi.org/10.1021/acs.cgd.4c00686
Cryst. Growth Des. 2024, 24, 7361−7388

(30) Lian, P.; Zhang, L.; Su, H.; Chen, J.; Chen, L.; Wang, J. A Novel Energetic Cocrystal Composed of CL-20 and 1-Methyl-2,4,5-Trinitroimidazole with High Energy and Low Sensitivity. *Acta Crystallogr. B Struct Sci. Cryst. Eng. Mater.* **2022**, *78* (2), 133−139.
(31) Yin, Y.; Wang, J.; Chen, J.; Sun, J.; Sui, H. Thermal Kinetics of Energetic CL-20/BTF Cocrystal Induced by Strong Intermolecular Coupling. *J. Phys. Chem. C* **2022**, *126* (19), 8199−8207.
(32) Tariq, Q.-N.; Bi, Y.; Manzoor, S.; Tariq, M.-N.; Cao, W.-L.; Dong, W.-S.; Zhang, J.-G. Synthesis, Performance, and Thermal Behavior of Two Insensitive 3,4-Dinitropyrazole-Based Energetic Cocrystals. *Cryst. Growth Des.* **2023**, *23* (1), 112−119.
(33) Risse, B.; Spitzer, D.; Pessina, F. Method For Producing Cocrystals by Means of Flash Evaporation. European Patent EP3164201, 2017.
(34) Liu, J.; Yan, Z.; Chi, D.; Yang, L. Synthesis of the Microspheric Cocrystal CL-20/2,4-DNI with High Energy and Low Sensitivity by a Spray-Drying Process. *New J. Chem.* **2019**, *43* (44), 17390−17394.
(35) Huang, C.; Xu, J.; Tian, X.; Liu, J.; Pan, L.; Yang, Z.; Nie, F. High-Yielding and Continuous Fabrication of Nanosized CL-20-Based Energetic Cocrystals via Electrospraying Deposition. *Cryst. Growth Des.* **2018**, *18* (4), 2121−2128.
(36) Levinthal, M. L. Propellant Made with Corystals of Cyclotetramethyenetetramine and Ammonium per Chlorate. U.S. Patent 4086110, April 25, 1978.
(37) Blas, L.; Klaumünzer, M.; Pessina, F.; Braun, S.; Spitzer, D. Nanostructuring of Pure and Composite-Based K6 Formulations with Low Sensitivities. *Propellants, Explosives, Pyrotechnics* **2015**, *40* (6), 938−944.
(38) Li, H.; An, C.; Guo, W.; Geng, X.; Wang, J.; Xu, W. Preparation and Performance of Nano HMX/TNT Cocrystals. *Propellants Explosives Pyrotechnics* **2015**, *40* (5), 652−658.
(39) Doblas, D.; Rosenthal, M.; Burghammer, M.; Chernyshov, D.; Spitzer, D.; Ivanov, D. Smart Energetic Nanosized Co-Crystals: Exploring Fast Structure Formation and Decomposition. *Cryst. Growth Des.* **2016**, *16* (1), 432−439.
(40) An, C.; Li, H.; Ye, B.; Wang, J. Nano-CL-20/HMX Cocrystal Explosive for Significantly Reduced Mechanical Sensitivity. *J. Nanomater.* **2017**, *2017*, 1−7.
(41) Stepanov, V.; Reddy, D.; Patel, R.; Qiu, H., Nanoscale Cocrystalline Explosives. U.S. PatentUS9790137B1, October 7, 2017.
(42) Liu, N.; Duan, B.; Lu, X.; Mo, H.; Xu, M.; Zhang, Q.; Wang, B. Preparation of CL-20/DNDAP Cocrystals by a Rapid and Continuous Spray Drying Method: An Alternative to Cocrystal Formation. *CrystEngComm* **2018**, *20* (14), 2060−2067.
(43) Gao, H.; Du, P.; Ke, X.; Liu, J.; Hao, G.; Chen, T.; Jiang, W. A Novel Method to Prepare Nano-sized CL-20/NQ Co-crystal: Vacuum Freeze Drying. *Propellants Explo Pyrotec* **2017**, *42* (8), 889−895.
(44) Li, Y.; Li, B.; Zhang, D.; Xie, L. Preparation and Characterization of a Series of High-Energy and Low-Sensitivity Composites with Different Desensitizers. *New J. Chem.* **2022**, *46* (11), 5218−5233.
(45) Viswanath, J. V.; Shanigaram, B.; Vijayadarshan, P.; Chowadary, T. V.; Gupta, A.; Bhanuprakash, K.; Niranjana, S. R.; Venkataraman, A. Studies and Theoretical Optimization of CL-20: RDX Cocrystal. *Prop., Explos., Pyrotech.* **2019**, *44* (12), 1570−1582.
(46) Shen, J. P.; Duan, X. H.; Luo, Q. P.; Zhou, Y.; Bao, Q.; Ma, Y. J.; Pei, C. H. Preparation and Characterization of a Novel Cocrystal Explosive. *Cryst. Growth Des.* **2011**, *11* (5), 1759−1765.
(47) Matzger, A.; Bolton, O. Crystalline Explosive Material. US 2012/0305150 A1, December 6, 2012.
(48) Bolton, O.; Simke, L.; Pagoria, P.; Matzger, A. High Power Explosive with Good Sensitivity: A 2:1 Cocrystal of CL-20:HMX. *Cryst. Growth Des.* **2012**, *12* (9), 4311−4314.
(49) Salan, J.; am Ende, J.; Anderson, S. R. CL-20:DNMT Cocrystal Crystal Structure. U.S. Patent US 2015/0361056A1, 2015.
(50) Xu, H.; Duan, X.; Li, H.; Pei, C. A Novel High-Energetic and Good-Sensitive Cocrystal Composed of CL-20 and TATB by a Rapid Solvent/Non-Solvent Method. *RSC Adv.* **2015**, *5* (116), 95764−95770.
(51) Qiu, H.; Patel, R. B.; Damavarapu, R. S.; Stepanov, V. Nanoscale 2CL-20·HMX High Explosive Cocrystal Synthesized by Bead Milling. *CrystEngComm* **2015**, *17* (22), 4080−4083.
(52) Anderson, S. R.; Dubé, P.; Krawiec, M.; Salan, J. S.; Ende, D. J. A.; Samuels, P. Promising CL-20-Based Energetic Material by Cocrystallization. *Prop., Explos., Pyrotech.* **2016**, *41* (5), 783−788.
(53) Song, X.; Wang, Y.; Zhao, S.; Li, F. Mechanochemical Fabrication and Properties of CL-20/RDX Nano Co/Mixed Crystals. *RSC Adv.* **2018**, *8* (59), 34126−34135.
(54) Liu, Y.; An, C.; Luo, J.; Wang, J. High-Density HNIW/TNT Cocrystal Synthesized Using a Green Chemical Method. *Acta Crystallographica Section B-Structural Science Crystal Engineering and Materials* **2018**, *74*, 385−393.
(55) Ghosh, M.; Sikder, A. K.; Banerjee, S.; Gonnade, R. G. Studies on CL-20/HMX (2:1) Cocrystal: A New Preparation Method and Structural and Thermokinetic Analysis. *Cryst. Growth Des.* **2018**, *18* (7), 3781−3793.
(56) Hu, Y.; Yuan, S.; Li, X.; Liu, M.; Sun, F.; Yang, Y.; Hao, G.; Jiang, W. Preparation and Characterization of Nano-CL-20/TNT Cocrystal Explosives by Mechanical Ball-Milling Method. *ACS Omega* **2020**, *5* (28), 17761−17766.
(57) Xue, Z.; Zhang, X.; Huang, B.; Cheng, J.; Wang, K.; Yang, Z.; Yan, Q. Assembling of Hybrid Nano-Sized HMX/ANPyO Cocrystals Intercalated with 2D High Nitrogen Materials. *Cryst. Growth Des.* **2021**, *21* (8), 4488−4499.
(58) Zohari, N.; Mohammadkhani, F.; Montazeri, M.; Roosta, S.; Hosseini, S.; Zaree, M. Synthesis and Characterization of a Novel Explosive HMX/BTNEN (2:1) Cocrystal. *Propellants Explosives Pyrotechnics* **2021**, *46* (2), 329−333.
(59) Herrmannsdörfer, D.; Klapötke, T. M. Semibatch Reaction Crystallization for Scaled-Up Production of High-Quality CL-20/HMX Cocrystal: Efficient Because of Solid Dosing. *Cryst. Growth Des.* **2021**, *21* (3), 1708−1717.
(60) Li, L.; Ling, H.; Tao, J.; Pei, C.; Duan, X. Microchannel-Confined Crystallization: Shape-Controlled Continuous Preparation of a High-Quality CL-20/HMX Cocrystal. *CrystEngComm* **2022**, *24* (8), 1523−1528.
(61) Qu, Y.; Qian, W.; Zhang, J.; Gong, F.; Xie, Z.; Yang, Z.; Nie, F.; Zhao, X. Interfacial Engineered RDX/TATB Energetic Co-Particles for Enhanced Safety Performance and Thermal Stability. *Dalton Trans.* **2022**, *51* (27), 10527−10534.
(62) Yang, F.; Yang, Z.; Yu, Q.; Li, G.; Zhao, C.; Tian, Y. "Thermal Escape" of MTNP: The Phase Separation of CL-20/MTNP Cocrystals under Long-Term Heating. *Phys. Chem. Chem. Phys.* **2023**, *25* (9), 6838−6846.
(63) Zhao, H.; Gu, G.; Shen, J.; Zhao, X.; Wang, J.; Lan, G. Preparation of Spherical HMX/DMF Solvates, Spherical HMX Particles, and HMX@NTO Composites: A Way to Reduce the Sensitivity of HMX. *ACS Omega* **2023**, *8* (15), 14041−14046.
(64) Yan, M.; Liu, Y.; Xu, J.; Yang, L.; Zhang, L.; Nie, F.; Huang, S. Porous Cyclotrimethylenetrinitramine with Reduced Sensitivity Prepared by a Solvation-Desolvation Method. *Cryst. Growth Des.* **2020**, *20* (8), 5387−5394.
(65) Tian, B.; Xiong, Y.; Chen, L.; Zhang, C. Relationship between the Crystal Packing and Impact Sensitivity of Energetic Materials. *CrystEngComm* **2018**, *20* (6), 837−848.
(66) Li, S.; Gou, R.; Zhang, C. N-π Stacking in Energetic Crystals. *Cryst. Growth Des.* **2022**, *22* (3), 1991−2000.
(67) Zhang, J.; Jin, B.; Peng, R.; Niu, C.; Xiao, L.; Guo, Z.; Zhang, Q. Novel Strategies for Synthesizing Energetic Materials Based on BTO with Improved Performances. *Dalton Transactions* **2019**, *48* (31), 11848−11854.
(68) Politzer, P.; Murray, J. S. Quantitative Analyses of Molecular Surface Electrostatic Potentials in Relation to Hydrogen Bonding and Co-Crystallization. *Cryst. Growth Des.* **2015**, *15* (8), 3767−3774.
(69) Ren, Z.; Chen, X.; Yu, G.; Wang, Y.; Chen, B.; Zhou, Z. Molecular Simulation Studies on the Design of Energetic Ammonium Dinitramide Co-Crystals for Tuning Hygroscopicity. *CrystEngComm* **2020**, *22* (31), 5237−5244.

https://doi.org/10.1021/acs.cgd.4c00686
Cryst. Growth Des. 2024, 24, 7361−7388

(70) Allen, F. H.; Baalham, C. A.; Lommerse, J. P. M.; Raithby, P. R.; Sparr, E. Hydrogen-Bond Acceptor Properties of Nitro-O Atoms: A Combined Crystallographic Database and Ab Initio Molecular Orbital Study. *Acta Cryst. B* **1997**, *53* (6), 1017−1024.
(71) Wei, X.; Ma, Y.; Long, X.; Zhang, C. A Strategy Developed from the Observed Energetic-Energetic Cocrystals of BTF: Cocrystallizing and Stabilizing Energetic Hydrogen-Free Molecules with Hydrogenous Energetic Coformer Molecules. *CrystEngComm* **2015**, *17* (37), 7150−7159.
(72) Wei, Y.; Ren, F.; Shi, W.; Zhao, Q. Theoretical Insight into the Influences of Molecular Ratios on Stabilities and Mechanical Properties, Solvent Effect of HMX/FOX-7 Cocrystal Explosive. *Journal of Energetic Materials* **2016**, *34* (4), 426−439.
(73) Vishnoi, P.; Walawalkar, M.; Murugavel, R. Containment of Polynitroaromatic Compounds in a Hydrogen Bonded Triarylbenzene Host. *Cryst. Growth Des.* **2014**, *14* (11), 5668−5673.
(74) Han, G.; Gou, R.; Ren, F.; Zhang, S.; Wu, C.; Zhu, S. Theoretical Investigation into the Influence of Molar Ratio on Binding Energy, Mechanical Property and Detonation Performance of 1,3,5,7-Tetranitro-1,3,5,7-Tetrazacyclo Octane (HMX)/1-Methyl-4,5-Dinitroimidazole (MDNI) Cocrystal Explosive. *Computational and Theoretical Chemistry* **2017**, *1109*, 27−35.
(75) Hao, L.; Wang, J.; Zhai, D.; Ma, P.; Ma, C.; Pan, Y.; Jiang, J. Theoretical Study on CL-20-Based Cocrystal Energetic Compounds in an External Electric Field. *ACS Omega* **2020**, *5* (24), 14767−14775.
(76) Chen, P.-Y.; Zhang, L.; Zhu, S.-G.; Cheng, G.-B. Intermolecular Interactions, Thermodynamic Properties, Crystal Structure, and Detonation Performance of CL-20/TEX Cocrystal Explosive. *Can. J. Chem.* **2015**, *93* (6), 632−638.
(77) Hang, G.; Yu, W.; Wang, T.; Wang, J.; Li, Z. Theoretical Insights into Effects of Molar Ratios on Stabilities, Mechanical Properties and Detonation Performance of CL-20/RDX Cocrystal Explosives by Molecular Dynamics Simulation. *J. Mol. Struct.* **2017**, *1141*, 577−583.
(78) Chen, R.; Aquino, A.; Sue, A.; Niehaus, T.; Lischka, H. Characterization of Charge Transfer in Excited States of Extended Clusters of Pi-Stacked Donor and Acceptor Complexes in Lock-Arm Supramolecular Ordering. *J. Phys. Chem. A* **2019**, *123* (21), 4532−4542.
(79) Şen, N. Characterization and Properties of a New Energetic Co-Crystal Composed of Trinitrotoluene and 2,6-Diaminotoluene. *J. Mol. Struct.* **2019**, *1179*, 453−461.
(80) Liu, Y.; Gou, R.; Zhang, S.; Chen, Y.-H.; Chen, M.-H.; Liu, Y.-B. Effect of Solvent Mixture on the Formation of CL-20/HMX Cocrystal Explosives. *J. Mol. Model* **2020**, *26* (1), 8.
(81) Bennion, J.; Vogt, L.; Tuckerman, M.; Matzger, A. Isostructural Cocrystals of 1,3,5-Trinitrobenzene Assembled by Halogen Bonding. *Cryst. Growth Des.* **2016**, *16* (8), 4688−4693.
(82) Bu, R.; Li, H.; Zhang, C. Polymorphic Transition in Traditional Energetic Materials: Influencing Factors and Effects on Structure, Property, and Performance. *Cryst. Growth Des.* **2020**, *20* (5), 3561−3576.
(83) Bolotina, N. B.; Hardie, M. J.; Speer, R. L., Jr; Pinkerton, A. A. Energetic Materials: Variable-Temperature Crystal Structures of γ- and ϵ-HNIW Polymorphs. *J. Appl. Crystallogr.* **2004**, *37* (5), 808−814.
(84) Zhang, L.; Yan, M.; Yin, W.; Li, J.; Liu, Y.; Zhao, S.; Huang, S. Experimental Study of the Crystal Habit of High Explosive Octahydro-1,3,5,7-Tetranitro-1,3,5,7-Tetrazocine (HMX) in Acetone and Dimethyl Sulfoxide. *Cryst. Growth Des.* **2020**, *20* (10), 6622−6628.
(85) Klasovitý, D.; Zeman, S.; Růžička, A.; Jungová, M.; Roháč, M. Cis-1,3,4,6-Tetranitrooctahydroimidazo-[4,5-d]Imidazole (BCHMX), Its Properties and Initiation Reactivity. *Journal of Hazardous Materials* **2009**, *164* (2−3), 954−961.
(86) Hakey, P.; Ouellette, W.; Zubieta, J.; Korter, T. Redetermination of Cyclo-Trimethylene-Trinitramine. *Acta Crystallographica Section E: Structure Reports Online* **2008**, *64* (8), o1428.
(87) Yang, Z.; Wang, Y.; Zhou, J.; Li, H.; Huang, H.; Nie, F. Preparation and Performance of a BTF/DNB Cocrystal Explosive. *Propellants, Explosives, Pyrotechnics* **2014**, *39* (1), 9−13.
(88) Zeng, Q.; Ma, Y.; Li, J.; Zhang, C. Energy Decomposition of Intermolecular Interactions in Energetic Co-Crystals. *CrystEngComm* **2017**, *19* (19), 2687−2694.
(89) Lu, F.; Dong, Y.; Fei, T.; Liu, J.; Su, H.; Li, S.; Pang, S. Noncovalent Modification of 4,4′-Azo-1,2,4-Triazole Backbone via Cocrystallization with Polynitroazoles. *Cryst. Growth Des.* **2019**, *19* (12), 7206−7216.
(90) Zhu, S.; Ji, J.; Zhu, W. Intermolecular Interactions, Vibrational Spectra, and Detonation Performance of CL-20/TNT Cocrystal. *J. Chin Chem. Soc.* **2020**, *67* (10), 1742−1752.
(91) Sultan, M.; Wu, J.; Haq, I. U.; Mudassar, M.; Yang, L.; Wu, J.; Lu, J.; Chen, L. A Complete Thermal Decomposition Mechanism Study of an Energetic-energetic CL-20/DNT Cocrystal at Different Extreme Temperatures by Using ReaxFF Reactive Molecular Dynamics Simulations. *J. Mol. Struct.* **2022**, *1269*, 133691.
(92) Liu, G.; Bu, R.; Huang, X.; Zhong, K.; Jiao, F.; Wei, S.-H.; Li, H.; Zhang, C. Energetic Cocrystallization as the Most Significant Crystal Engineering Way to Create New Energetic Materials. *Cryst. Growth Des.* **2022**, *22* (2), 954−970.
(93) Liu, G.; Li, H.; Gou, R.; Zhang, C. Packing Structures of CL-20-Based Cocrystals. *Cryst. Growth Des.* **2018**, *18* (11), 7065−7078.
(94) Ma, Y.; Zhang, A.; Zhang, C.; Jiang, D.; Zhu, Y.; Zhang, C. Crystal Packing of Low-Sensitivity and High-Energy Explosives. *Cryst. Growth Des.* **2014**, *14* (9), 4703−4713.
(95) Bu, R.; Xiong, Y.; Zhang, C. π-π Stacking Contributing to the Low or Reduced Impact Sensitivity of Energetic Materials. *Cryst. Growth Des.* **2020**, *20* (5), 2824−2841.
(96) Zhang, J.; Shreeve, J. Time for Pairing: Cocrystals as Advanced Energetic Materials. *Cryst. Growth Des.* **2016**, *18* (33), 6124−6133.
(97) Duan, B.; Shu, Y.; Liu, N.; Wang, B.; Lu, X.; Lu, Y. Direct Insight into the Formation Driving Force, Sensitivity and Detonation Performance of the Observed CL-20-Based Energetic Cocrystals. *CrystEngComm* **2018**, *20* (38), 5790−5800.
(98) Şen, N.; Dursun, H.; Hope, K. S.; Nazir, H.; Acar, N.; Atakol, O. Towards Low-Impact-Sensitivity through Crystal Engineering: New Energetic Co-Crystals Formed between Picric Acid, Trinitrotoluene and 9-Vinylanthracene. *J. Mol. Struct.* **2020**, *1219*, 128614.
(99) Hanafi, S.; Trache, D.; Meziani, R.; Boukciat, H.; Mezroua, A.; Tarchoun, A. F.; Derradji, M. Synthesis, Characterization and Thermal Decomposition Behavior of a Novel HNTO/AN Co-Crystal as a Promising Rocket Propellant Oxidizer. *Chemical Engineering Journal* **2021**, *417*, 128010.
(100) Guo, C.; Zhang, H.; Wang, X.; Xu, J.; Liu, Y.; Liu, X.; Huang, H.; Sun, J. Crystal Structure and Explosive Performance of a New CL-20/Caprolactam Cocrystal. *J. Mol. Struct.* **2013**, *1048*, 267−273.
(101) Chapman, C. J.; Groven, L. J. Evaluation of a CL-20/TATB Energetic Co-Crystal. *Prop., Explos., Pyrotech.* **2019**, *44* (3), 293−300.
(102) Zhao, L.; Yin, Y.; Sui, H.; Yu, Q.; Sun, S.; Zhang, H.; Wang, S.; Chen, L.; Sun, J. Kinetic Model of Thermal Decomposition of CL-20/HMX Co-Crystal for Thermal Safety Prediction. *Thermochim. Acta* **2019**, *674*, 44−51.
(103) Huang, B.; Xue, Z.; Fu, X.; Yan, Q.-L. Advanced Crystalline Energetic Materials Modified by Coating/Intercalation Techniques. *Chemical Engineering Journal* **2021**, *417*, 128044.
(104) Guo, D.; An, Q.; Zybin, S. V.; Goddard, W. A., Iii; Huang, F.; Tang, B. The Co-Crystal of TNT/CL-20 Leads to Decreased Sensitivity toward Thermal Decomposition from First Principles Based Reactive Molecular Dynamics. *J. Mater. Chem. A* **2015**, *3* (10), 5409−5419.
(105) Wu, X.; Liu, Z.; Zhu, W. Conformational Changes and Decomposition Mechanisms of HMX-Based Cocrystal Explosives at High Temperatures. *J. Phys. Chem. C* **2020**, *124* (1), 25−36.
(106) (a) Patil, V. B.; Svoboda, R.; Zeman, S. Thermal Studies on Performance of DATB and TATB Coagglomerated Crystals. *Thermochimica Acta* **2023**, *724*, 179494. (b) Zeman, S.; Yan, Q.-L.; Vlček, M. Recent Advances in the Study of the Initiation of Energetic Materials using Characteristics of Their Thermal Decomposition. Part I, Cyclic Nitramines. *Central European Journal of Energetic Materials* **2014**, *11* (2), 173−189.

https://doi.org/10.1021/acs.cgd.4c00686
Cryst. Growth Des. 2024, 24, 7361−7388

(107) Pang, W.-q.; Wang, K.; Zhang, W.; Luca, L. T. D.; Fan, X.-z.; Li, J.-q. CL-20-Based Cocrystal Energetic Aterials: Simulation, Preparation and Performance. *Molecules* **2020**, *25* (18), 4311.
(108) Patil, V. B.; Zalewski, K.; Schuster, J.; Belina, P.; Trzcinski, W.; Zeman, S. A New Insight into the Energetic Co-Agglomerate Structures of Attractive Nitramines. *Chemical Engineering Journal* **2021**, *420*, 130472.
(109) Zhang, Z.-B.; Li, T.; Yin, L.; Yin, X.; Zhang, J.-G. A Novel Insensitive Cocrystal Explosive BTO/ATZ: Preparation and Performance. *RSC Adv.* **2016**, *6* (79), 76075−76083.
(110) Vuppuluri, V. S.; Samuels, P. J.; Caflin, K. C.; Gunduz, I. E.; Son, S. F. Detonation Performance Characterization of a Novel CL-20 Cocrystal Using Microwave Interferometry. *Prop., Explos., Pyrotech.* **2018**, *43* (1), 38−47.
(111) Vuppuluri, V. S.; Bennion, J. C.; Wiscons, R. A.; Gunduz, I. E.; Matzger, A. J.; Son, S. F. Detonation Velocity Measurement of a Hydrogen Peroxide Solvate of CL-20. *Prop., Explos., Pyrotech.* **2019**, *44* (3), 313−318.
(112) Wahler, S.; Klapötke, T. M. Research Output Software for Energetic Materials Based on Observational Modelling 2.1 (RoseBoom2.1©). *Materials Advances* **2022**, *3* (21), 7976−7986.
(113) Bolton, O.; Simke, L. R.; Pagoria, P. F.; Matzger, A. J. High Power Explosive with Good Sensitivity: A 2:1 Cocrystal of CL-20:HMX. *Cryst. Growth Des.* **2012**, *12* (9), 4311−4314.
(114) Tan, Y.; Liu, Y.; Wang, H.; Li, H.; Nie, F.; Yang, Z. Different Stoichiometric Ratios Realized in Energetic-Energetic Cocrystals Based on CL-20 and 4,5-MDNI: A Smart Strategy to Tune Performance. *Cryst. Growth Des* **2020**, *20*, 3826−3833.
(115) Yadav, A. K.; Ghule, V. D.; Dharavath, S. Thermally Stable and Insensitive Energetic Cocrystals Comprising Nitrobarbituric Acid Coformers. *Cryst. Growth Des.* **2023**, *23* (4), 2826−2836.
(116) Peng, P.; Ding, N.; Zhao, C.; Li, Y.; Liu, J.; Li, S.; Pang, S. Improving the Stability of All-Carbon-Nitrated Azoles through Cocrystallization. *Cryst. Growth Des.* **2022**, *22* (4), 2158−2167.
(117) Abdelaziz, A.; Tarchoun, A.; Boukeciat, H.; Trache, D. Insight into the Thermodynamic Properties of Promising Energetic HNTO·AN Co-Crystal: Heat Capacity, Combustion Energy, and Formation Enthalpy. *Energies* **2022**, *15* (18), 6722.
(118) Qiao, S.; Wang, J.; Yu, Y.; Liu, Y.; Yang, Z.; Li, H. Two Novel TNB Energetic Cocrystals with Low Melting Point: A Potential Strategy to Construct Melt Cast Explosive Carriers. *CrystEngComm* **2022**, *24* (16), 2948−2953.
(119) Duan, B.; Lu, X.; Mo, H.; Tan, B.; Wang, B.; Liu, N. Fabrication of CL-20/HMX Cocrystal@Melamine-Formaldehyde Resin Core-Shell Composites Featuring Enhanced Thermal and Safety Performance via In Situ Polymerization. *IJMS* **2022**, *23* (12), 6710.
(120) Jia, Q.; Zhang, J.; Zhang, S.; Shi, Q.; Lei, D.; Xu, Y.; Kou, K. Low-Temperature Heat Capacities, Standard Molar Enthalpies of Formation and Detonation Performance of Two CL-20 Cocrystal Energetic Materials. *Fluid Phase Equilib.* **2020**, *518*, 112638.
(121) Ren, C.; Li, X.; Guo, L. Chemical Insight on Decreased Sensitivity of CL-20/TNT Cocrystal Revealed by ReaxFF MD Simulations. *J. Chem. Inf. Model.* **2019**, *59* (5), 2079−2092.
(122) Zeman, S.; Hussein, A. K.; Jungova, M.; Elbeih, A. Effect of Energy Content of the Nitraminic Plastic Bonded Explosives on Their Performance and Sensitivity Characteristics. *Defence Technology* **2019**, *15* (4), 488−494.
(123) McBain, A.; Vuppuluri, V.; Gunduz, I.; Groven, L.; Son, S. Laser Ignition of CL-20 (Hexanitrohexaazaisowurtzitane) Cocrystals. *Combust. Flame* **2018**, *188*, 104−115.
(124) Wang, H.; Liu, Y.; Liu, Q.; Kang, Y.; Yuan, M.; An, M.; Gao, H.; Zhang, Q.; Wang, Y. Hydrogen Bonding Distribution and Its Effect on Sensitivity of Planar Tricyclic Polyazole Energetic Materials. *Chemical Engineering Journal* **2022**, *433*, 134479.
(125) O'Sullivan, O. T.; Zdilla, M. J. Properties and Promise of Catenated Nitrogen Systems As High-Energy-Density Materials. *Chem. Rev.* **2020**, *120* (12), 5682−5744.
(126) Lin, H.; Zhu, S.-G.; Zhang, L.; Peng, X.-H.; Li, H.-Z. Synthesis and First Principles Investigation of HMX/NMP Cocrystal Explosive. *Journal of Energetic Materials* **2013**, *31* (4), 261−272.
(127) Lin, H.; Zhu, S.-G.; Zhang, L.; Peng, X.-H.; Chen, P.-Y.; Li, H.-Z. Intermolecular Interactions, Thermodynamic Properties, Crystal Structure, and Detonation Performance of HMX/NTO Cocrystal Explosive. *Int. J. Quantum Chem.* **2013**, *113* (10), 1591−1599.
(128) Zhang, L.; Jiang, S.-L.; Yu, Y.; Chen, J. Revealing Solid Properties of High-Energy-Density Molecular Cocrystals from the Cooperation of Hydrogen Bonding and Molecular Polarizability. *Sci. Rep* **2019**, *9* (1), 1257.
(129) Zhang, H.; Guo, C.; Wang, X.; Xu, J.; He, X.; Liu, Y.; Liu, X.; Huang, H.; Sun, J. Five Energetic Cocrystals of BTF by Intermolecular Hydrogen Bond and π-Stacking Interactions. *Cryst. Growth Des.* **2013**, *13* (2), 679−687.
(130) Wu, X.; Liu, Z.; Zhu, W. External Electric Field Induced Conformational Changes as a Buffer to Increase the Stability of CL-20/HMX Cocrystal and Its Pure Components. *Materials Today Communications* **2021**, *26*, 101696.
(131) Zhou, J.-H.; Zhao, L.; Shi, L.-W.; Luo, P.-C. Two Models to Estimate the Density of Organic Cocrystals. *RSC Adv.* **2021**, *11* (20), 12066−12073.
(132) Jia, Q.; Wang, J.; Zhang, S.; Zhang, J.; Liu, N.; Kou, K. Investigation of the Solid-Liquid Ternary Phase Diagrams of 2HNIW·HMX Cocrystal. *RSC Adv.* **2021**, *11* (16), 9542−9549.
(133) Yang, Z.; Li, H.; Huang, H.; Zhou, X.; Li, J.; Nie, F. Preparation and Performance of a HNIW/TNT Cocrystal Explosive. *Propellants, Explosives, Pyrotechnics* **2013**, *38* (4), 495−501.
(134) Zeman, S. The Chemical Micromechanism of Energetic Material Initiation. In *Nano and Micro-Scale Energetic Materials*; John Wiley & Sons, Ltd, 2023; pp 567−623, DOI: 10.1002/9783527835348.ch19.
(135) Dlott, D. D. Multi-Phonon up-Pumping in Energetic Materials. In *Overviews of Recent Research on Energetic Materials*; Advanced Series in Physical Chemistry; WORLD SCIENTIFIC, 2005; Vol. *16*, pp 303−333, DOI: 10.1142/9789812775283_0010.
(136) Qian, W.; Zhang, C. Review of the Phonon Calculations for Energetic Crystals and Their Applications. *Energetic Materials Frontiers* **2021**, *2* (2), 154−164.
(137) Zeman, S. Characteristics of Thermal Decomposition of Energetic Materials in a Study of Their Initiation Reactivity. In *Handbook of Thermal Analysis and Calorimetry*; Elsevier, 2018; Vol. *6*, pp 573−612, DOI: 10.1016/B978-0-444-64062-8.00006-1.
(138) Suceska, M. *Test Methods for Explosives*; Springer Science & Business Media, 2012.
(139) Zeman, S. Sensitivities of High Energy Compounds. In *High Energy Density Materials*; Klapötke, T. M., Ed.; Structure and Bonding; Springer: Berlin, Heidelberg, 2007; pp 195−271, DOI: 10.1007/430_2006_052.
(140) Licht, H.-H. Performance and Sensitivity of Explosives. *Propellants Explos. Pyrotech* **2000**, *25* (3), 126−132.
(141) Zeman, S.; Jungová, M. Sensitivity and Performance of Energetic Materials. *Propellants Explo Pyrotec* **2016**, *41*, 426.
(142) Bao, S.-Y.; Zeng, W.; Liu, F.-S.; Liu, Z.-T.; Liu, Q.-J. Theoretical Relationship between Vibrational Properties and Impact Sensitivity of Energetic Materials from the Phonon upon Transition Theory. *Chem. Phys.* **2024**, *576*, 112085.
(143) Ren, H.-C.; Ji, L.-X.; Chen, T.-N.; Jia, X.-Z.; Liu, R.-P.; Zhang, X.-Q.; Wei, D.-Q.; Wang, X.-F.; Ji, G.-F. Intermolecular Vibration Energy Transfer Process in Two CL-20-Based Cocrystals Theoretically Revealed by Two-Dimensional Infrared Spectra. *Molecules* **2022**, *27* (7), 2153.
(144) Zeman, S.; Liu, N. A New Look on the Electric Spark Sensitivity of Nitramines. *Defence Technology* **2020**, *16* (1), 10−17.
(145) Xu, H.; Duan, X.; Li, H.; Pei, C. A Novel High-Energetic and Good-Sensitive Cocrystal Composed of CL-20 and TATB by a Rapid Solvent/Non-Solvent Method. *RSC Adv.* **2015**, *5* (116), 95764−95770.

(146) Bidault, X.; Chaudhuri, S. Can a Shock-Induced Phonon up-Pumping Model Relate to Impact Sensitivity of Molecular Crystals, Polymorphs and Cocrystals? *RSC Adv.* **2022**, *12* (48), 31282−31292.
(147) McNesby, K. L.; Coffey, C. S. Spectroscopic Determination of Impact Sensitivities of Explosives. *J. Phys. Chem. B* **1997**, *101* (16), 3097−3104.
(148) Tarver, C. M. Multiple Roles of Highly Vibrationally Excited Molecules in the Reaction Zones of Detonation Waves. *J. Phys. Chem. A* **1997**, *101* (27), 4845−4851.
(149) Bernstein, J. *Ab Initio* Study of Energy Transfer Rates and Impact Sensitivities of Crystalline Explosives. *J. Chem. Phys.* **2018**, *148* (8), 084502.
(150) Zhang, C.; Jiao, F.; Li, H. Crystal Engineering for Creating Low Sensitivity and Highly Energetic Materials. *Cryst. Growth Des.* **2018**, *18* (10), 5713−5726.
(151) Gruhne, M.; Lommel, M.; Wurzenberger, M.; Klapotke, T.; Stierstorfer, J. Investigation of Ethylenedinitramine as a Versatile Building Block in Energetic Salts, Cocrystals, and Coordination Compounds. *Inorg. Chem.* **2021**, *60* (7), 4816−4828.
(152) Hussein, A. K.; Elbeih, A.; Zeman, S. The Effect of Glycidyl Azide Polymer on the Stability and Explosive Properties of Different Interesting Nitramines. *RSC Adv.* **2018**, *8* (31), 17272−17278.
(153) Xu, X.; Zhang, R.; Xia, W.; Ma, P.; Ma, C.; Pan, Y.; Jiang, J. Density Functional Theory Study of CL-20/Nitroimidazoles Energetic Cocrystals in an External Electric Field. *Computational and Theoretical Chemistry* **2022**, *1209*, 113607.
(154) Hang, G.; Wang, J.; Wang, T.; Shen, H.; Yu, W.; Shen, R. Theoretical Investigations on Stability, Sensitivity, Energetic Performance, and Mechanical Properties of CL-20/TNAD Cocrystal Explosive by Molecular Dynamics Method. *J. Mol. Model* **2022**, *28* (3), 58.
(155) Auzanneau, M.; Roux, M. Electric Spark and ESD Sensitivity of Reactive Solids (Primary or Secondary Explosive, Propellant, Pyrotechnics). Part II: Energy Transfer Mechanisms and Comprehensive Study on E50. *Propellants, Explosives, Pyrotechnics* **1995**, *20* (2), 96−101.
(156) Zeman, S.; Pelikan, V.; Majzlik, J. Electric Spark Sensitivity of Nitramines. Part I. Aspects of Molecular Structure. *Central European Journal of Energetic Materials* **2006**, *3* (3), 27−44.
(157) Zeman, S.; Pelikan, V.; Majzlik, J. Electric Spark Sensitivity of Nitramines. Part II. A Problem of "Hot Spots". *Central European Journal of Energetic Materials* **2006**, *3* (3), 45−51.
(158) Fried, L E. *CHEETAH 1.39 Users' Manual*, UCRL-MA-117541; Lawrence Livermore National Laboratory, 1996.
(159) Liouville, P. J. Sur la propagation des réactions chimiques dans les gaz. *J. Math. Pures Appl.* **1906**, *2*, 5−86.
(160) Kamlet, M. J.; Jacobs, S. J. Chemistry of Detonations. I. A Simple Method for Calculating Detonation Properties of C-H-N-O Explosives. *J. Chem. Phys.* **1968**, *48* (1), 23−35.
(161) Urbanski, T. On Entropy and Free Energy of Explosives (Preliminary Communication). *Bull. Acad. Pol. Des Sci.* **1980**, *28*, 511−513.
(162) Lin, H.; Zhu, S.-G.; Li, H.-Z.; Peng, X.-H. Structure and Detonation Performance of a Novel HMX/LLM-105 Cocrystal Explosive. *J. Phys. Org. Chem.* **2013**, *26* (11), 898−907.
(163) Wu, J.-T.; Zhang, J.-G.; Li, T.; Li, Z.-M.; Zhang, T.-L. A Novel Cocrystal Explosive NTO/TZTN with Good Comprehensive Properties. *RSC Adv.* **2015**, *5* (36), 28354−28359.
(164) Hang, G.-Y.; Yu, W.-L.; Wang, T.; Wang, J.-T. Theoretical Investigations on Structures, Stability, Energetic Performance, Sensitivity, and Mechanical Properties of CL-20/TNT/HMX Cocrystal Explosives by Molecular Dynamics Simulation. *J. Mol. Model* **2019**, *25* (1), 10.
(165) Sha, Y.; Zhang, X. Impact Sensitivity and Moisture Adsorption on the Surface of CL-20/TNT Cocrystal by Molecular Dynamics Simulation. *Appl. Surf. Sci.* **2019**, *483*, 91−97.
(166) Song, K.; Ren, F.; Zhang, S.; Shi, W. Theoretical Insights into the Stabilities, Detonation Performance, and Electrostatic Potentials of Cocrystals Containing α- or β-HMX and TATB, FOX-7, NTO, or DMF in Various Molar Ratios. *J. Mol. Model* **2016**, *22* (10), 249.
(167) Pakhnova, M.; Kruglov, I.; Yanilkin, A.; Oganov, A. Search for Stable Cocrystals of Energetic Materials Using the Evolutionary Algorithm USPEX. *Phys. Chem. Chem. Phys.* **2020**, *22* (29), 16822−16830.
(168) Aakeröy, C. B.; Wijethunga, T. K.; Desper, J. Crystal Engineering of Energetic Materials: Co-Crystals of Ethylenedinitramine (EDNA) with Modified Performance and Improved Chemical Stability. *Chem.—Eur. J.* **2015**, *21* (31), 11029−11037.
(169) Bellas, M. K.; Matzger, A. J. Achieving Balanced Energetics through Cocrystallization. *Angew. Chem., Int. Ed.* **2019**, *58* (48), 17185−17188.
(170) Patil, V. B.; Yan, Q.-L.; Trzciński, W. A.; Bělina, P.; Shánělová, J.; Musil, T.; Zeman, S. Co-Agglomerated Crystals of Cyclic Nitramines with Sterically Crowded Molecules. *CrystEngComm* **2022**, *24*, 7771.
(171) Patil, V. B.; Bělina, P.; Trzcinski, W. A.; Zeman, S. Preparation and Properties of Co-Mixed Crystals of 1,3-Di- and 1,3,5-Tri-Amino-2,4,6-Trinitrobenzenes with Attractive Cyclic Nitramines. *Journal of Industrial and Engineering Chemistry* **2022**, *115*, 135−146.
(172) Patil, V. B.; Bělina, P.; Trzcinski, W. A.; Zeman, S. Co-Agglomerated Crystals of 2,2′,4,4′,6,6′-Hexanitro-Stilbene/-Azobenzene with Attractive Nitramines. *Chemical Engineering Journal* **2023**, *457*, 141200.
(173) Patil, V. B.; Svoboda, R.; Zeman, S. Towards the Thermal Reactivity and Behavior of Co-Agglomerated Crystals of DATB and TATB with Attractive Nitramines. *Thermochim. Acta* **2023**, *724*, 179494.
(174) Patil, V. B.; Bělina, P.; Trzcinski, W. A.; Zeman, S. Co-Agglomerated Crystals of Cyclic Nitramines with the Nitrogen Rich 3,6-Bis(1H-1,2,3,4-Tetrazol-5-Ylamino)-1,2,4,5-Tetrazine (BTATz). *Chemical Engineering Journal* **2024**, *483*, 149029.
(175) Patil, V. B. Achieving balanced co-crystals of energetic materials by co-agglomeration and their application. Ph.D. Thesis, University of Pardubice, Czech Republic, 2024; pp 8−224.
(176) Cobbledick, R. E.; Small, R. W. H. The Crystal Structure of the δ-Form of 1,3,5,7-Tetranitro-1,3,5,7-Tetraazacyclooctane (δ-HMX). *Acta Cryst. B* **1974**, *30* (8), 1918−1922.
(177) Patil, V. B.; Machalický, O.; Svoboda, R.; Trzcinski, W. A.; Zeman, S.; Bělina, P. Co-Agglomerated - Polyaniline Composite Crystals of Attractive Nitramines. *Composites, and Hybrid materials* **2024**, *7*, 125.
(178) Zhang, H.; Liu, Y.; Li, S.; Huang, S.; Xu, J.; Zhang, H.; Li, J.; Yang, S. Three-Dimensional Hierarchical 2,2,4,4,6,6-Hexanitrostilbene Crystalline Clusters Prepared by Controllable Supramolecular Assembly and Deaggregation Process. *CrystEngComm* **2016**, *18* (41), 7940−7944.
(179) Zeman, S. The Influence of Energy Content and Its Outputs on the Impact Sensitivity of High-Nitrogen Energetic Materials, Journal of Energetic Materials. *Journal of Energetic Materials* **2022**, *40* (1), 1−14.
(180) Zeman, S.; Jungová, M. Sensitivity and Performance of Energetic Materials. *Propellants, Explosives, Pyrotechnics* **2016**, *41* (3), 426−451.
(181) Patil, V. B.; Zeman, S. Novel Approach for Preparation of the Energy-Safety Balanced Cocrystals of Attractive Nitramines *via* Coagglomeration. *FirePhysChem.* **2024**, *4*, 283.
(182) Novák, M. *Ověření Vlivu Bicyklo-HMX Na Parametry Prachu s Obsahem RDX (Verification of the Bicyclo-HMX Effect on the RDX Gunpowder Parameters), The Final Project of the Licensing Study*; Univ. Pardubice, 2022
(183) Hussein, A.; Elbeih, A.; Zeman, S. Performance Characteristics of a New Plastic Explosive Based on Cis-1,3,4,6-Tetranitrooctahydroimidazo-[4,5-d]Imidazole (BCHMX) and 3-Nitro-1,2,4-Triazol-5-One(NTO). In *NTREM 2017*; University of Pardubice: Czech Republic, 2017; Vol. *20*.
(184) Patil, V. B.; Bělina, P.; Trzcinski, W. A.; Zeman, S. Co-Agglomerated Crystals of Cyclic Nitramines with the Nitrogen Rich 3,6-Bis(1H-1,2,3,4-Tetrazol-5-Ylamino)-1,2,4,5-Tetrazine (BTATZ). **2023**. *Chemical Engineering Journal Chemistry* **2024**, *483*, 149029.

https://doi.org/10.1021/acs.cgd.4c00686
Cryst. Growth Des. 2024, 24, 7361−7388

(185) Kolla, H. S.; Surwade, S. P.; Zhang, X.; MacDiarmid, A. G.; Manohar, S. K. Absolute Molecular Weight of Polyaniline. *J. Am. Chem. Soc.* **2005**, *127* (48), 16770−16771.
(186) Ou, Y.; Wang, C.; Pan, Z.; Chen, B. Sensitivity of Hexanitrohexaazaisowurtzitane. *HanNeng CaiLiao (Chin. J. Energet. Mater.)* **1999**, *7*, 100−108.

https://doi.org/10.1021/acs.cgd.4c00686
Cryst. Growth Des. 2024, 24, 7361−7388